

RICE UNIVERSITY

A FUNDAMENTAL STUDY OF SPRAY EVAPORATIVE COOLING

by

William M. Grissom

A THESIS SUBMITTED
IN PARTIAL FULFILLMENT OF THE
REQUIREMENTS FOR THE DEGREE OF

Master of Science

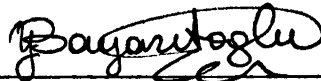
APPROVED, THESIS COMMITTEE:



Frederic A. Wierum, Professor
Thesis Director



Alan J. Chapman, Professor



Yildiz Bayazitoglu, Assistant Professor

Houston, Texas

May, 1979

ABSTRACT

"Spray evaporative cooling" is defined as the mode of spray cooling heat transfer for which no liquid film would form on a heated surface of infinite extent. The heat flux during this mode is simply that required to vaporize all of the impinging spray.

The lower surface temperature range limit for the existence of spray evaporative cooling is determined experimentally to be an essentially linear function of the impinging spray mass flux. This suggests a conduction-controlled droplet evaporation mechanism. An analytical model of this form gives fairly good agreement with the experimental measurements at atmospheric pressure.

The effect of lowering the surrounding pressure appears to be a decreased "wettability" of the liquid (distilled water) upon the aluminum surface. This would account for the correspondingly lower droplet evaporation times observed.

"Spray film cooling" is defined as the mode of spray cooling heat transfer for which a liquid film would exist upon the heated surface. An analysis of this mode is of importance in determining several characteristics of the spray evaporative cooling mode.

At atmospheric pressure the mechanism governing spray film cooling appears to be quite similar to that of ordinary pool boiling with little or no dependence upon the liquid film thickness. At vacuum pressures spray film cooling appears to be governed by the simple mechanism of heat conduction through the liquid film, and very much dependent upon the liquid film thickness.

The "Leidenfrost State" is defined as the mode in which impinging

droplets rebound off of the surface. The initiation of the Leidenfrost state imposes the upper range limit for the existence of spray evaporative cooling. The surface temperature at which this state is initiated is found to be very much a function of the surrounding pressure. Interestingly, this variation with pressure is such that it counteracts the variation of the lower range limit with pressure, resulting in essentially the same maximum possible heat flux during spray evaporative cooling for all surrounding pressures.

ACKNOWLEDGMENT

The author is especially grateful to the Crew Systems Division of the National Aeronautics and Space Administration - Johnson Space Center, which funded the research presented here through NASA Grant NAS9-65274. Their understanding, particularly that of Louis Trevino, Contract monitor, when the research required a much more fundamental investigation than originally anticipated is especially acknowledged.

Professor Frederic A. Wierum, Principal Investigator for the grant and Thesis Director, showed undying enthusiasm throughout the research project. His guidance through the experimental research and thesis preparation is appreciated.

A note of thanks is due the Electrical Engineering and Geology departments at Rice for their aid in loaning several instruments during the reserach.

Finally, a word of thanks to the departmental secretary Marla Wells who typed the final manuscript and kept track of all of the paperwork throughout the project.

TABLE OF CONTENTS

	<u>Page</u>
ACKNOWLEDGMENTS	i
LIST OF FIGURES AND TABLES	iii
NOMENCLATURE	v
I. INTRODUCTION	1
II. PREVIOUS RESEARCH	3
III. ANALYSIS	5
IV. EXPERIMENTAL PROCEDURE	11
A. Heat flux measurements	11
B. Spray characteristics	13
C. Temperature control	14
D. Unsteady measurements	16
E. Vacuum system	17
F. Spray film cooling	19
V. DATA ANALYSIS	21
VI. EXPERIMENTAL RESULTS AND ANALYSIS	23
A. Flooding locus measurements	23
B. Spray film cooling data	28
C. Leidenfrost state temperature	30
D. Droplet size measurements	31
E. Overall range of spray evaporative cooling	32
VII. CONCLUSIONS	35
APPENDIX A: ANALYTICAL ANALYSIS	36
APPENDIX B: ANALYSIS OF SURFACE CONDUCTIVITY EFFECTS	48
APPENDIX C: ENERGY BALANCE AT THE DROPLET SURFACE	50
REFERENCES	52

LIST OF FIGURES AND TABLES

	<u>Page</u>
Figure 1. Operation of NASA's "Flash Evaporator System"	57
Figure 2. The three modes of operation during spray cooling	58
Figure 3. Mechanism during transition from drywall to flooded modes	58
Figure 4. Predictions of the "Analysis"	59
Figure 5. Schematic diagram of the heat flux sample	60
Figure 6. Effects of varying spray parameters upon total mass striking surface	61
Figure 7. Original temperature control circuit	62
Figure 8. Schematic diagram of vacuum system and liquid spray	63
Figure 9. Measurements of the flooding locus at atmospheric pressure	64
Figure 10. Summary of all spray evaporative cooling measurements to date	65
Figure 11. Measured flooding locus for $\bar{P} = 6.76$ mmHg	66
Figure 12. The effect of surrounding pressure changes upon the flooding locus	67
Figure 13. h^* as a function of \bar{T}_s	68
Figure 14. Spray film cooling curve compared with flooding curve, atmospheric pressure	69
Figure 15. Spray film measurements using orifice #2	70
Figure 16. Droplet size distributions	71
Figure 17. Overall spray evaporative cooling range at atmospheric pressure	72
Figure 18. Simplified model for thermal conductivity analysis	73
Figure 19. Initial droplet shape	74
Figure 20. Droplet during second domain of evaporation	74
Figure 21. Effect of mass removal at droplet surface upon thickness	74

LIST OF FIGURES AND TABLES

	<u>Page</u>
Table 1. Data analysis computer program	75
Photos 1-4. Construction of heat flux sample	80
Photo 5. Thermocouple measuring apparatus	81
Photo 6. Temperature control circuit	81
Photos 7,8. Vacuum System	81

NOMENCLATURE

A_o	=	initial area of droplet on surface
\bar{A}	=	time-weighted average droplet area
A_t	=	total average area for droplet evaporation
A_x	=	area reduction factor
b	=	spatially averaged thickness of droplet on surface
b_o	=	initial average droplet thickness
C_p	=	specific heat of spray fluid
d	=	initial diameter of spherical droplet
\bar{d}_v	=	mass-weighted average spherical droplet diameter
D	=	"spread diameter" of droplet on surface
D_o	=	initial spread diameter
\bar{D}	=	time-weighted average spread diameter
h^*	=	flooding coefficient
K	=	thermal conductivity of spray fluid
K_{Al}	=	thermal conductivity of aluminum
K_m	=	thermal conductivity of surface material
\dot{m}	=	spray mass flux impinging on surface
m	=	coefficient in relation $b = d^m$
n	=	$1 + 2p$ = convenient grouping of terms
p	=	$1/2 (3/m-1)$ = coefficient in relation $b = D^p$
P	=	surrounding pressure (absolute)
\bar{P}	=	average surrounding pressure for all measurements with a given orifice
q	=	surface heat flux
q^*	=	surface heat flux required to vaporize all impinging spray mass flux

- q_m^* = maximum surface heat flux possible for the dry-wall state
 t = time measured from beginning of second domain in analytical analysis
 T = temperature within evaporating droplet
 T_o = initial temperature of spray fluid
 T_{Al} = temperature within aluminum heat flux sample
 T_b = surface temperature at which spray film cooling heat flux exceeds spray evaporative heat flux
 T_f = surface temperature at which flooding state is initiated
 T_s = saturation temperature of spray fluid
 \bar{T}_s = saturation temperature corresponding to \bar{P}
 T_v = surface temperature at which Leidenfrost state is initiated
 T_w = surface temperature at any time
 x = distance measurement from surface, always positive
 α = thermal diffusivity of spray fluid
 θ = $T - T_s$
 θ_w = $T_w - T_s$
 λ = latent heat of vaporization of spray fluid
 λ^* = $\lambda + C_p (T_s - T_o)$ = augmented latent heat
 ρ = specific heat of spray fluid
 τ = time measured from droplet impact with surface
 τ_1 = time τ at the end of first domain
 τ_2 = time t at the end of second domain
 τ_t = $\tau_1 + \tau_2$ = total droplet evaporation time
 ϕ = contact angle of spray fluid on surface

I. INTRODUCTION

There are many industrial situations in which a fine liquid spray contacts a surface which is at a temperature in excess of the liquid saturation temperature. The term "spray cooling" will be used to describe this process.

In most such situations the transfer of heat from the surface is the desired effect. In other cases it is a secondary effect, subserviant to other design considerations. It may even be an undesirable side effect, to be avoided, in still other situations.

The purpose of the research reported in this thesis is to indentify the fundamental heat transfer processes involved in spray cooling, to provide experimental data useful to the design engineer, and to add to the general understanding of the overall spray cooling process.

The particular application of spray cooling which provided the impetus for the present research was in the operation of the novel heat exchanger system known as the "Flash Evaporator System" which has been selected by the National Aeronautics and Space Administration (NASA) for use as part of the enviromental control system in the Space Shuttle (see Figure 1).

In this unique application expendable liquids are sprayed as a fine mist on the interior walls of a heat exchanger. The walls are heated by the coolant in the environmental control system heat rejection loop. The pressure within the heat exchanger is maintained near the triple point of the spray liquid in order that the lowest possible liquid saturation temperatures may be

realized. The evaporation of the mist at the walls requires the transfer of considerable heat to the liquid to supply the large latent heat of vaporization.

Other applications of spray cooling are encountered in steam generator boiler tubes ^{(1-3)*} in which water droplets in the two phase flow diffuse to the walls, in the fuel injection and vaporization process in internal combustion engines ⁽⁴⁻⁶⁾, in the cooling of turbine blades ⁽⁷⁾, in such cryogenic applications as the freeze-drying of foods ⁽⁸⁻¹²⁾, in the spray cooling of hot metals in the steel industries ⁽¹³⁾, in the spray drying of liquid process streams ^(14,15), and in liquid metal heat transfer systems encountered mainly in the nuclear power industries ^(16,17).

*Numbers in superscripts () indicate references listed at the end of the thesis

II. PREVIOUS RESEARCH

Despite the myriad applications described in the previous section, little research effort has been devoted to understanding the detailed heat transfer mechanisms involved in the spray cooling process. It is believed that the bulk of the previous publications have been located during the present research.

Three distinct operational modes of spray cooling can be identified. The first is the case in which the surface vaporizes all of the impinging spray. This will be referred to as the "dry-wall" state and the term "spray evaporative cooling" will be used to describe the heat transfer process in this mode. One previous researcher has concentrated on the overall process in this mode (18, 19) while others have considered the mechanics of the evaporation of a single droplet (20,21).

The second operational mode is that in which the spray forms a thin liquid film upon the surface. This will be referred to as the "flooded" state and the term "spray film cooling" will be employed to describe the associated heat transfer process. Several previous studies have concentrated on this mode of heat transfer (22-31).

The final operational mode is that in which the impinging droplets are deflected from the surface by a thin vapor film which forms on impact. This will be referred to as the "Leidenfrost" state in recognition of the first researcher to investigate the phenomenon. There have been rather extensive studies of the Leidenfrost mode of heat transfer (7, 32-46).

Most of the previous research investigations of the first two modes of heat transfer (the dry-wall and flooded states) have been of a very empirical nature with the aim of simply defining that transfer coefficients.

It will be seen later that for the present range of heat fluxes considered here, the studies of the Leidenfrost phenomenon will not be directly applicable. Bonacina's experimental work ⁽¹⁸⁾ establishes the necessary background, while elements of Toda's extensive research ⁽²²⁾ are applicable.

III. ANALYSIS

In order to lay the groundwork for an experimental investigation, a detailed analysis of the three modes of spray cooling heat transfer is necessary.

Consider the case of a moderate spray impinging on a surface at a temperature somewhat in excess of the liquid saturation temperature (Figure 2). Under the proper conditions the surface temperature can be such that the droplets on the surface are evaporated faster than the arrival of the next droplets (Figure 2c). This is the dry-wall mode, characterized by spray evaporative cooling.

The heat flux during spray evaporative cooling is related very simply to the spray mass flux by the first law of thermodynamics. Assuming no superheating of the departing vapor:

$$q = \dot{m}\lambda^* \quad (1)$$

With the heat transfer during spray evaporative cooling so simply expressed it is seen that what is of interest is the range over which it may exist. To determine this range is the fundamental problem of spray evaporative cooling and is the question addressed in this thesis.

Suppose now that with the spray unchanged, the surface temperature is lowered. At some point one should reach the case of the surface temperature being too low to evaporate the droplets any faster than they arrive (Figure 2b). At a sufficiently lower surface temperature one would realize the second mode of spray

cooling heat transfer that of spray film cooling in which a thin liquid film covers the entire surface (Figure 2a).

The heat transfer process during spray film cooling should be very much akin to that in pool boiling. Above a certain wall temperature nucleate boiling within the film should occur.

The characteristics of the spray should be generally unimportant during the flooded mode. Indeed one investigator⁽⁴⁷⁾ found that even supplying the liquid as a thin jet affected only the burnout and not the heat transfer below burnout.

Below the nucleate boiling temperature the heat transfer through the film would be a conduction and free convection process. The liquid film thickness in this case might be a very important parameter.

Above the nucleate boiling temperature the liquid film thickness should not be as significant. For a film thickness much larger than the diameters of the vapor bubbles generated at the wall the process might be validly modeled as one of an infinite liquid film thickness (pool boiling).

Consider now the possible mechanics of the transition between the dry-wall and flooded states. When the surface just begins to "flood" at the temperature T_f (Figure 3a), small masses of fluid or "pools" begin to form on the surface. Two distinct situations may result depending upon whether the heat flux through the small "pools" is greater or less than the heat flux through the surface to the surrounding droplets.

Case A: (see figure 3B and 4)

If the small pools "hinder" the overall heat transfer through

the surface then not all of the spray mass can be evaporated (Eq. 1) resulting in some mass accumulating on the surface.

Each increase in the pool size would further decrease the surface heat flux, increasing still further the rate of mass accumulation. The result would be a catastrophic change to the flooded state, all at the surface temperature T_f (Figure 3c).

Mass would continue collecting indefinitely or it would run off of the surface in a manner determined by the geometry of the surface. Nothing in general may be said about the resulting liquid film thickness and hence the heat transfer.

To return the surface to its previously dry-wall state the surface temperature must be raised in excess of T_f until such time that the heat transfer through the thin film equals that required by Equation 1 to vaporize all of the impinging spray mass flux. This is a hysteresis effect which is not often observed in thermal systems.

Case B: (see Figures 3d and 4)

If, on the other hand, the small pools "aid" the overall heat transfer through the surface then a stable condition would result.

Each decrease in the surface temperature below T_f would increase the pool size. But this increased pool size would in turn increase the heat transfer rate to offset the decreased surface temperature. At some surface temperature well below T_f the surface would finally be covered completely by a thin liquid film. No "run off" would occur at this point (Figure 3e).

For further surface temperature decreases the heat transfer rate would begin to decrease, as described by the spray film cooling curve, and mass would then begin to run off of the surface.

As to which of these cases will result it is difficult to predict a priori. Assume for the present that the small droplets are evaporated from their surface entirely, with no boiling within the droplets. This would be essentially a conduction limited phenomenon and as such the heat flux would be roughly linear with temperature difference.

For T_w less than the nucleate boiling temperature the same case would hold within the thin liquid film of the small pools. However, being much larger than the droplets the pools should have a much larger thermal resistance. This should guarantee that Case A would result for T_w less than the nucleate boiling temperature.

As T_w is increased past the nucleate boiling temperature the heat flux through the small pools would increase as a power function of the temperature difference $T_w - T_s$. At some temperature T_b it should exceed the linearly increasing heat flux to the spray droplets. For $T_w \geq T_b$ then, Case B should result (see Figure 4).

Although the effort here was not to study spray film cooling in detail, a spray film cooling curve for the surface-liquid pair used here was necessary to determine when each of the above cases would result once surface flooding was initiated.

Consider now the other range limit for spray evaporative cooling - the initiation of the Leidenfrost state.

At a sufficiently high surface temperature T_v , an impinging droplet would begin to vaporize at the bottom as it contacted the

surface. This would quickly spread into a vapor film which would allow for a partially inelastic collision with the surface, resulting in the droplet rebounding off of the surface on impact (Figure 2d).

In the case of a small heat transfer surface area, most of the droplets which bounce off of the surface would never strike it again. All of the previous research has been for this configuration.

For the case of a surface of "infinite" extent however, all of the droplets which rebound off of the surface must land again at another point on the surface. Analogous to the previous argument, when the surface heat flux falls below that dictated by Equation 1 mass must begin collecting on the surface. In this case the liquid film which formed might very well be in a film boiling state.

This formation of a vapor film under an impinging droplet decreases the surface heat flux so dramatically that for the range of mass fluxes considered here, the initiation of the Leidenfrost state on a surface of infinite extent would lead immediately to a flooded surface.

The heat transfer during the Leidenfrost state, then, is of little importance for spray evaporative cooling considerations. What is of overriding importance is the determination of the surface temperature at which the Leidenfrost state is initiated.

Referring to Figure 4, it can be seen that the crux of an experimental analysis rests upon determining the locus of flooding points for spray evaporative cooling. These yield the maximum possible heat flux for each surface temperature during this mode

of heat transfer. Of interest also is the determination of the Leidenfrost state temperature T_v , which specifies the uppermost range for spray evaporative cooling, q_m^* .

The influence of several parameters upon these curves is of considerable interest. The effects of decreases in the surrounding pressure were studied here for water at a constant supply temperature sprayed through a given nozzle onto a polished aluminum surface.

A priori one might assume that the only effect of surrounding pressure changes would be to change the saturation temperature of the liquid. It will be seen later that this does not appear to be the case.

It might be added here that one feature of spray evaporative cooling of possible interest to a design engineer would be the ability to specify very accurately a surface heat flux (Eq. 1). This requires a knowledge of the impinging spray mass flux, but this is a rather easily measured quantity for a given nozzle and surface orientation.

IV. EXPERIMENTAL PROCEDURE

A. Heat flux measurements

From the "Analysis" it was concluded that the two main variables to measure are the surface temperature and the heat flux. A very common technique was employed to do this.

Shown in Figure 5 is a schematic of the heat flux sample. From nine copper-constantan thermocouples (1-9) the temperature profile within the 6061-T6 aluminum cylinder was found, from which both the temperature and temperature gradient at the surface were evaluated. Two additional thermocouples (10,11) located near the surface verified that a one-dimensional profile exists.

The thermocouples were located 1/4" apart in 1/16" diameter holes, the first located 1/4" below the surface. They were formed using Leeds & Northrup "Quicktip" thermocouple connectors. The wires were of the standard two-wire pair. Wood's metal (M.P. 80°C) was inserted in the tips of the holes to insure excellent thermal contact. All terminal connections were submerged in oil to avoid moisture contamination.

Thermocouple outputs were measured with a millivolt potentiometer (L&N #8662). An oil-submerged reference thermocouple in a well-insulated ice bath provided the reference voltage. The end result was the ability to measure temperatures within 0.3°C.

Thermal leakages were calculated to be small. The effect of any leakages, being axisymmetric, would be only to limit the maximum heat flux possible, they would not affect the measurement of the temperature and temperature gradient at the surface. Convective

losses at the surface were calculated to be on the order of 0.1 - 1% of the measured heat flux.

Even though distilled water was used for the spray fluid, the surface would be covered with a very thin film of contaminants after each run. This was removed by polishing with 00 grade steel wool prior to each run.

Heat was supplied by a 400W commercial cartridge heater (Chromalox CIR-3020). A method of adjusting the voltage to the heater was a major consideration in the experiment.

Thermal leakages out of the base were much higher than anticipated. The maximum possible heat flux obtained at atmospheric pressure was only 70% of design. Operation at vacuum pressures drastically curtailed these losses as a result of the lack of a convective environment. This allowed maximum heat fluxes of about 90% of design to be obtained.

Both the thermocouple nearest the surface and the one farthest from the surface were recorded on a chart recorder (Heath-Schlumberger model SR-206 2 pen recorder). This allowed continuous monitoring of the thermal conditions and an indispensable record of each experimental run.

Photos 1-3 show the construction of the heat flux sample with the thermocouple wiring running through grooved channels in the teflon insulation. Photo 4 shows the assembled heat flux sample with resistance heater inserted at the base and the spray collection funnel at the top. The entire assembly is placed upon the vacuum system base plate. Photo 5 shows the thermocouple switch, ice point,

and potentiometer.

An additional thermocouple was constructed to act as a surface temperature probe. Being handheld it was difficult to maintain the proper pressure to obtain a steady reading. A further problem was that droplets collecting on the tip would run onto the surface disturbing the steady-state established in the aluminum sample. The use of this device was soon abandoned.

B. Spray characteristics

In an attempt to determine the possible control variables, the characteristics of the spray were investigated. The amount of liquid striking the surface was measured in a sample jar with an entrance of the same diameter as the metal surface.

The spray was supplied at 25°C through a 0.4 mm D, 45° included angle, full cone nozzle. Pressure was supplied by applying the 60 psia output of an air pressure regulator to distilled water in a 9 gallon low-pressure storage vessel. The flow rate was adjusted with a needle valve and measured with a ball-in-tube rotameter. The measured flow rate was of use as an indirect measurement only.

The results for the case of the spray nozzle positioned directly over the surface are given in Figure 6. It is seen that changes in the total flow rate through the nozzle have an unpredictable effect upon the amount of water striking the surface. Height changes have a monotonic effect upon the amount of mass striking the surface. But this variable cannot be controlled for low pressure runs under a bell jar.

The decision was made to use the thermal variables - heat input or surface temperature - as the control variables, leaving the spray conditions unchanged throughout a run. This has the somewhat undesirable penalty that thermal changes require a much longer delay before the result is observed at the surface, whereas spray changes yield an almost instantaneous change at the surface.

C. Temperature control

The independent variable described in the "Analysis" was the surface temperature. For electrical heating, heat flux is the usual independent variable. The difficulty in specifying the heat flux rather than the surface temperature is easily explained.

For a given spray mass flux under dry-wall conditions there is only one surface heat flux (given by Eq. 1) which may result. If more heat than this is applied, the surface temperature will simply increase without bound. If less heat is applied the metal sample will cool continuously until the surface temperature falls below T_f and the surface floods. Steady-state operation is then not possible using heat input as the independent variable.

To specify a constant temperature instead, one of the thermocouple outputs is used as a sensor in a feedback control circuit. Initially the on-off circuit of Figure 7 was constructed (Photo 6). Later this was replaced by a commercial temperature controller which used a mechanical relay (Omega Model 49T).

The thermocouple located closest to the heater (No. 9) was used as the sensor to provide the fastest time response. The control

circuit altered the reading from this thermocouple so it was not used in most of the data measurements.

The only controllers available seem to work in the on-off mode rather than a truly proportional mode. This is due to the difficulty in controlling such large AC currents with a small DC input. Consequently very steady temperature control is difficult, a hysteresis of 2°C not being uncommon. The optimum temperature control was obtained by adjusting the supply voltage to where it was just slightly in excess of that required to vaporize all of the impinging spray. The "on-off" controller then remained "on" for a much longer percentage of the time.

The procedure using temperature control was as follows. With the surface in the dry-wall state the spray nozzle was positioned approximately 45 cm above the surface at a flow rate of 100 cc/min. It was turned angularly until the surface just began to flood, then backed off slightly to maintain the surface in the dry-wall state.

The set point to the temperature controller was then lowered gradually at discrete intervals of approximately 5 minutes, allowing a steady-state to be reached after each small change. When the surface just barely began collecting liquid pools the thermocouple outputs were measured and the data point recorded.

For high heat fluxes the spray generally pointed straight down at the surface, while for the lower heat fluxes only the fringe of the spray was used, with the nozzle axis at approximately 45°

with the horizontal. The assumption was made that droplet characteristics were constant across the spray cone. As will be seen later there was a significant difference in the droplet diameter distributions between the center of the spray and the fringe. The average droplet diameter, however, remained essentially constant across the spray cone.

D. Unsteady measurement

An alternate method to that of using feedback temperature control to specify a temperature was to adjust the heat input until it was just slightly less than the heat taken out of the surface by the evaporating spray. With the high heat fluxes realized, a 1 volt ($\sim 4\text{w}$) change would have a significant increase or decrease in the rate of cooling of the metal.

By careful trial and error, the proper heat flux for a given spray could be found such that the rate of cooling of the aluminum sample was slow enough that an almost linear temperature profile existed within the aluminum. To ensure that all of the thermocouples were read before the temperature decreased significantly, either a portable digital voltmeter (Data Precision Model 248) or a digital thermometer (Omega Model 2809) were used in place of the potentiometer (which required some time to balance for each reading). The former instrument required calibration with the potentiometer prior to a series of readings, whereas the latter always agreed within 0.01 mV of the potentiometer readings.

The procedure otherwise was equivalent to that in the temperature controlled method. With practice this came to be the preferred

method, due mainly to the rapidity with which data could be collected. This was especially true for low pressure data, as the temperature controller became even more unstable at the correspondingly lower thermocouple output voltages.

E. Vacuum System

The vacuum system consisted of an 18 in. diameter, 30 in. high glass bell jar with stainless steel base plate. Wire and fluid passages were provided through the base plate⁽⁵¹⁾. A large liquid nitrogen cold trap froze the vapor generated. This protected the vacuum pump from condensates and provided a "vapor pump" effect. A schematic of the overall system is shown in Figure 8. The total system is shown in Photos 7 and 8.

An orifice plate placed in the exit duct from the bell jar "choked" the exiting vapor flow. This insured that back pressure fluctuations from the vacuum pump were not propagated to the bell jar test chamber. By using different size orifices the pressure under the bell jar could be maintained within different distinct pressure ranges.

Pressures were measured by either a diaphragm pressure gauge (MKS Instruments "Baratron" 0-100 μ m Hg), a McLeod gauge (Stokes 0-500 μ m Hg), or a single tube manometer Merium 0-250 mm Hg). All gave the same reading when in overlapping ranges. The pressure connections were continually tested for leaks by closing off the connection of the bell jar and noting the rate of increase of pressure in the pressure tap lines.

It was predicted that the atmosphere under the bell jar would be at saturated conditions. To test this, two thermometers

were placed where part of the spray would wet the bulbs. They always read the saturation temperature at the measured pressure. Hence this direct measurement of the saturation temperature was used when possible.

Other than being under a bell jar where manual manipulation of the nozzle was impossible the experimental procedure at vacuum pressures was identical to that at atmospheric pressure. It was difficult to predict ahead of time how much spray would strike the surface as the spray pattern was quite different at vacuum pressures. Experience aided greatly here.

The spray pattern appeared to be essentially a hollow cone at these vacuum pressures. It was often necessary to adjust the flow rate through the nozzle to obtain a uniform spray distribution over the surface. There is the possibility then that droplet characteristics might be quite different for different nozzle flow rates. It has been suggested, however, that the droplet diameters for injection into a vacuum environment are fairly uniform, regardless of nozzle conditions, due to the spontaneous "explosions" of the droplets to a diameter small enough that the surface tension provides an internal pressure large enough to prevent the production of vapor within the droplet.

Collection of the large quantity of the spray not striking the surface and evaporating was aided by the placement of a large collection bucket above the aluminum surface. The remainder was collected below the spray collection funnel through a runoff tube.

Three different orifices were used to provide three distinct pressure ranges. Orifice No. 3 (5/8"D) provided a range just

slightly below the triple point pressure of water (4.59 mm Hg), while orifice No. 2 (3/8"D) provided a pressure range slightly above the triple point.

Orifice No. 1 (1/8"D) was to provide a pressure range as close to atmospheric pressure as possible. The goal was to test the effect of relative humidity upon the spray evaporative cooling process, the atmosphere under the bell jar having a relative humidity of 100%. This required an extremely small orifice (1/32"D), however. This size made initial pump-down of the bell jar extremely difficult. The 1/8 inch diameter was found to provide the best compromise.

For a given orifice the pressure would increase slightly for higher heat fluxes since more vapor was generated. However, since only about 20% of the vapor came from that generated at the aluminum surface, this effect was rather slight.

The greatest difficulty came with operation below the triple point pressure. At these pressures the only thermodynamic equilibrium state possible is with either ice or vapor. After approximately 5 minutes of operation enough ice would have collected on the insulated surfaces to block some of the spray from striking the aluminum surface. This made experimentation very difficult as repeated "shutdowns" to remove the ice were necessary.

F. Spray film cooling

Below the burnout point, the region of interest here, boiling imposes a steady state upon the system. That is, for an imposed heat flux the surface temperature will increase or decrease until it is such that the heat flux through the surface balances the imposed heat flux. This is a result of q being a monotonically

increasing function of $T_w - T_s$ over this range.

A boiling curve for each test pressure, then, was readily obtained. The procedure was simply to impose a heat flux and allow the system to reach steady state. This was done for several heat fluxes to obtain a well correlated curve. The spray was adjusted such that the flooded state existed with only a minimum amount of runoff from the surface.

V. DATA ANALYSIS

To obtain the temperature profile within the aluminum sample a parabolic least-squares line was fitted through the thermocouple readings. This was actually an emf vs. distance curve since the thermocouple mV readings were used directly to fit the curve.

The projected emf reading at the surface was then evaluated and converted to temperature using the most recent National Bureau of Standards copper-constantan tables. The surface heat flux was found as:

$$q|_{\text{surface}} = k_{al} \left. \frac{dT_{al}}{dx} \right|_{x=0} = k_{al} (T_W) \left. \frac{d(\text{emf})}{dx} \right|_{x=0} \left. \frac{\Delta T}{\Delta \text{emf}} \right|_{T_W} \quad (2)$$

Precise data on the conductivity of 6061-T6 aluminum was not available. The most consistently listed current value is (48)

$$0.167 \frac{\text{kw}}{\text{M} - ^\circ\text{C}} \quad (96.7 \text{ Btu/hr-ft-}^\circ\text{F})$$

Values 8% lower than this have been listed⁽⁴⁹⁾. No data on the variation with temperature is given. If the variation is assumed to be the same as that for pure aluminum⁽⁵⁰⁾, an approximate expression (with T in $^\circ\text{F}$) yields:

$$k_{al}(T) = 92.82 + 8.184 \cdot 10^{-2} - 4.144 \cdot 10^{-4} T^2 \text{ Btu/hr-ft-}^\circ\text{F} \quad (3)$$

With all errors included it was generally possible to determine

the surface temperature within 0.6°C ($\pm 2\%$ range) while the surface heat flux could be determined within 10 kw/m^2 ($\pm 3\%$ range). A special run was made measuring the heat flux and comparing with the mass collected in the sampling jar. An 8% difference was noted which might easily have been due to the difficulty in repositioning the nozzle over the sample jar.

A listing of the computer program used to carry out the data analysis is given in Table 1. The program performed the least squares curve fit and interpolated in the T vs. emf tables for copper-constantan thermocouples and the P vs. T_s tables for water. All properties which vary with temperature (K , $\Delta T/\Delta E$, λ) were calculated as such.

All data points were originally plotted to insure that no erroneous readings were present. The temperature profiles determined were linear in almost all instances. The computer program simply improved upon the calculated heat fluxes and surface temperatures determined from these plots.

VI. EXPERIMENTAL RESULTS AND ANALYSIS

A. Flooding locus measurements

In Figure 9 the atmospheric measurements of the flooding temperature for a given mass flow rate (or corresponding heat flux) are given. To obtain these data points all of the atmospheric data was carefully judged by reviewing the chart paper records of each run and questionable measurements were eliminated.

The data points which were discarded were either taken during experimental runs performed before the final procedure, test conditions, and measuring instruments were established or were taken while significant fluctuations in surface conditions existed. They were generally recorded simply to obtain some measurement for an otherwise unfruitful run.

The remaining "good" experimental measurements plotted in Figure 9 display a fairly good correlation. Only one data point deviates significantly from the rest and there is an indication on the chart paper record of this run that the surface was still above the flooding temperature when it was recorded.

The scatter in the data is due primarily to the difficulty in providing a very stable spray mass flux to the surface. At the very large heat fluxes associated with the process, the thermal capacitance of the aluminum sample was not sufficient to attenuate the temperature fluctuations ($\sim 0.1\text{Hz}$) caused by the spray mass flux fluctuations to a satisfactory level. Surface temperature fluctuations of 4°C were not uncommon during an

atmospheric run. Producing a very constant spray mass flux at the surface is of primary importance in obtaining very accurate experimental measurements.

There is no indication that the scatter is due to any unknown parameter being different between experimental runs. Several measurements were taken one after the other as the surface temperature was repeatedly brought to the flooding temperature, the spray conditions remaining constant during the procedure. The scatter between these data points was generally indicative of the overall scatter in Figure 9.

The "best fit" line drawn through the data of Figure 9 requires some defense. It is drawn linearly in the high heat flux region, intersecting the origin. The deviation of the measurements from this linear fit in the vicinity of the origin is attributed here to a mass transfer effect.

It is known from thermodynamics that a liquid will evaporate to an unsaturated atmosphere at any temperature above the "wet bulb" temperature. This is the case here, as the "wet bulb" temperature was generally about 15.5°C with a relative humidity of about 50%. At the higher heat fluxes the atmosphere directly over the evaporating droplets probably becomes almost saturated with the large amount of vapor generated. Hence the resulting linear flooding locus in this region.

It might be added here that three very steady measurements were taken in the center region of Figure 9. They are not shown, however, because unfortunately the thermocouple ice point was not refilled prior to the run. Between them they yield almost the

very same shape as the fitted curve. Their relative position with respect to the temperature axis is, however, undeterminable.

In Figure 10 all of the atmospheric measurements taken during this study are presented along with the only known measurements by other researchers. It is necessarily a logarithmic plot to include the wide range of Bonacina's measurements.

As discussed previously in the "Analysis" a physically realizable steady state may exist during the dry-wall mode at any point to the right of the flooding loci (but below the Leidenfrost state temperature). This is shown very well in Figure 10. The flooding locus line is that determined from Figure 9. Most measurements lie near this line since this was the state to be determined.

Bonacina (18,19) does not state directly the characteristics of the surface state during his measurements. He indicates, however, that many of his measurements may have been in the partially flooded region (Case B of Figure 4). This may be especially true of his very high heat flux measurements.

The majority of the low pressure experimentation was carried out using the medium sized orifice (number 2). This provided a pressure range just slightly above the triple point of water (4.59 mm Hg). The other two orifice plates were used with the intention of testing the effect of perturbations from this pressure range.

The results of the measurements of the flooding locus using orifice no. 2 are given in Figure 11. For the most part the data shows much better correlation than that taken at atmospheric pressure. No effort towards ruling out certain data points

was warranted.

The better correlations appear to be due to a much steadier spray mass flux. This is probably a result of the very sparse atmosphere under the bell jar which does not greatly disturb droplets in transit to the surface.

The three poorly correlated measurements in the low heat flux range (which were the first measurements taken at low pressure) can be explained with reference to Figure 4. For a surface temperature above the flooding temperature yet below the spray film cooling temperature for the present heat flux, a potentially unstable situation exists.

If a small pool of liquid is deposited upon the surface the heat transfer through the pool will not be sufficient to vaporize all of the spray striking the top of the pool. The pool will then grow gradually until it covers the entire surface, all of this occurring at a surface temperature in excess of the flooding temperature.

In the present case drops of liquid collecting on the teflon surface surrounding the heat flux surface flow onto the surface at times, initiating this phenomenon. This appears to have been the situation which precipitated these three poorly correlated measurements.

In Figure 12 the results for the pressure ranges provided by orifice No. 1 and 3 are compared with the results from the orifice No. 2 and the atmospheric experimentation (Figures 9 and 11). There appears to be a very significant change in the flooding locus curve with pressure.

The results of the runs with orifice no. 1 are very well correlated with only one point deviating significantly from the other measurements. This data point apparently was the result of the same phenomenon which precipitated the first three erroneous measurements with orifice no. 2.

As described in the "Experimental Procedure", experimentation with orifice no. 3 was greatly complicated by the formation of ice on the insulated surfaces when the pressure was below the triple point. This was the case with all but the three at the highest heat fluxes. The scatter in the orifice No. 3 measurements is generally due to these complications.

Since the pressures realized using orifice no. 3 were only slightly below the triple point, the problem of determining the saturation temperature for this non-equilibrium thermodynamic state of liquid and vapor was not really encountered. It is suggested here that, in the absence of other data, extrapolation of the T_s vs. P curve below the triple point is the favored course, the alternative being to use the solid-vapor sublimation curve.

Since the pressures realized for each orifice varied over the range of measurements with that orifice, an average pressure is used to identify the pressure realized with that orifice. This yields:

Orifice #1 18-23 mmHg, $\bar{P} = 19$ mmHg, $\bar{T}_s = 21.3^\circ\text{C}$

Orifice #2 4.8-13.0 mmHg, $\bar{P} = 6.76$ mmHg, $\bar{T}_s = 5.28^\circ\text{C}$

Orifice #3 4.3-4.65 mmHg, $\bar{P} = 4.56$ mmHg, $\bar{T}_s = 0^\circ\text{C}$

Atmospheric $\bar{P} = 1$ atm $\bar{T}_s = 100^\circ\text{C}$

The results of Figures 9, 11, and 12 may be more easily compared

by defining a "flooding coefficient":

$$h^* = \frac{q^*}{(T_f - T_s)} \quad (4)$$

This is simply the slope of the flooding locus for each orifice. The results are presented in Figure 13.

An analytical analysis for the atmospheric case, given in Appendix A, yields $h^* = 18 \text{ kw/m}^2 \text{ } ^\circ\text{C}$. This is 17% higher than the experimentally determined value but is still within the error limits of the experimental measurements.

Although similar to a heat transfer coefficient, h^* cannot generally be applied in the same manner. Its usage implies only that

$$q^* \sim (T_f - T_s) \quad (5)$$

h^* is applied in the following manner. To realize the dry-wall state for a given mass flux \dot{m} , with the heat flux given as:

$$q^* = \dot{m}\lambda^* \quad (1)$$

T_W must be such that:

$$T_s + \dot{m}\lambda^*/h^* < T_W < T_v \quad (6)$$

B. Spray film cooling data

The spray film cooling measurements at atmospheric pressure

are given in Figure 14, compared with the flooding locus curve of Figure 9.

The data taken as a continuous set shows very good correlation. The other measurements were taken during spray evaporative cooling runs after the surface had become flooded.

The conditions under which the different measurements were taken varied widely. There does not appear to have been any influence upon the heat flux by such variations as the liquid film thickness, supply rate, etc.

In Figure 15, spray film cooling measurements using orifice No. 2 are presented. Curve (a) consists of measurements taken with the nozzle very close to the surface, which provided a very thin liquid film. Curve (b) consists of measurements in which the liquid film was supplied by steadily dripping liquid onto the surface, which provided a fairly thick liquid film. Measurements taken during spray evaporative cooling runs just after the surface had flooded show a very wide range of values and are not presented here.

The spray film cooling mechanism at vacuum pressure appears to be distinctly different from that at atmospheric pressure. Rather than possessing a nucleate boiling region it appears to be a totally conduction controlled phenomenon, very much dependent upon the liquid film thickness.

Visual observations noted that the liquid film would continually "explode" at these vacuum pressures. No nucleate bubble formation was ever observed. The ability of the liquid to wet the surface appeared to be drastically altered as well. The liquid behaved as if there was a "waterproof" coating upon the aluminum surface.

It was somewhat difficult to maintain a liquid film over the total surface area.

Since no measurements of the liquid film thickness at these vacuum pressures were performed (and it would be a difficult measurement to make) no general correlation of the spray film cooling measurements for this pressure range (4.8-13 mmHg) are presented. It is hypothesized that a very simple one-dimensional conduction model:

$$R_{th} = \frac{T}{k} \quad (8)$$

where T = liquid film thickness, might be entirely adequate to predict the heat transfer rate for this situation.

C. Leidenfrost state temperature

It was not the intention of the present study to perform a detailed study of the Leidenfrost state. It is quite important, however, to determine the Leidenfrost state temperature, T_v , in order to specify the upper range limit for spray evaporative cooling. This would also permit a determination of q_m^* in Figure 4.

Several rather quick measurements were performed to obtain an estimate of the initiation of the Leidenfrost state. At atmospheric pressure a single measurement determined:

$$T_v - T_s = 38 \pm 14^\circ\text{C}, P = 1 \text{ atm}$$

while Zodrow (52) determined

$$T_v - T_s = 39 \pm 6^\circ\text{C}, P = 1 \text{ atm}$$

Several more careful measurements at vacuum pressures using orifice No. 2 determined:

$$T_v - T_s = 78 \pm 6^\circ\text{C}, \bar{P} = 6.76 \text{ mmHg } (\bar{T}_s = 5.75^\circ\text{C})$$

The majority of the references in the literature on the Leidenfrost phenomenon are concerned with the initiation of stable film boiling underneath a rather large sessile drop. This temperature, defined as the "Leidenfrost Point" is generally around 200°C above saturation for water. It does not seem to predict at all when a small impinging droplet will bounce off of the surface.

D. Droplet size measurements

The droplet size should be an important variable in the spray evaporative cooling mechanics. For this reason a determination of the droplet size distributions over the spray cone at atmospheric pressure was attempted.

The measurements were performed by simply collecting droplets on an oil film and measuring the resulting droplet diameters with an optical microscope. The assumption was that the droplets would assume a spheroidal shape upon the oil film. The results for two locations in the nozzle spray - (1) center of spray and (2) fringe of spray - are given in Figure 16.

What is of importance is the mass weighted average droplet diameter, \bar{d}_v . This was obtained by making a plot of droplet volume

distribution and determining the average droplet volume, from which \bar{d}_v follows directly:

$$\bar{d}_{v1} = 182\mu\text{m}, \bar{d}_{v2} = 127\mu\text{m}$$

Since all atmospheric measurements were performed between the two spray regions measured, the average diameter for all atmospheric measurements was taken as the average of \bar{d}_{v1} and \bar{d}_{v2} :

$$\bar{d}_v = 155 \mu\text{m}$$

Perhaps the only means of determining the size of the droplets at the vacuum pressures would be photographically. This was not attempted here. From observations of the droplet sizes on the aluminum surface they appeared to be of the same order of magnitude as those at atmospheric pressure.

E. Overall range of spray evaporative cooling

If the linear evaporation mechanism is assumed to continue for approximately three times the range considered here then the overall spray evaporative cooling range would be as shown in Figure 17. The maximum possible heat flux, q_m^* may be calculated as:

$$q_m^* = 590 \pm 150 \text{ kw/m}^2 @ P = 1 \text{ atm}$$

For vacuum pressure operation with orifice No. 2 q_m^* may be calculated as

$$q_m^* = 485 \pm 125 \text{ kw/m}^2 \text{ @ } \bar{P} = 6.76 \text{ mmHg}$$

Due to the conduction mechanism through a liquid film, no spray film cooling curve may be drawn for vacuum pressure operation in general.

It appears that in spite of significant changes in h^* and $T_v - T_s$ with pressure, the quantity $q_m^* = h^* (T_v - T_s)$ remains essentially the same. The effect of pressure changes then appears to be a "stretching" of the temperature coordinate.

That the physics of the process would predict this is questionable. A satisfactory physical explanation would be that the apparently decreased "wettability" of the aluminum surface at vacuum pressures affects both h^* and $(T_v - T_s)$ to the same degree.

This would imply that both h^* and $T_v - T_s$ depend upon the contact angle in the same manner. For a power law dependence upon ϕ :

$$h^* \sim 1/\phi^{\text{power}}$$

and

$$T_v - T_s \sim \phi^{\text{power}}$$

Study of the effects of pressure upon contact angles would be needed to answer these questions.

q_m^* is the maximum heat flux possible for which an entirely dry-wall state may be maintained at the surface. It is possible to operate in the partially-flooded mode described in the "Analysis" (Case B). Operation in this partially-flooded mode would still

insure that all of spray mass flux is vaporized and would permit operation to heat fluxes as high as the spray film cooling "burnout" heat flux.

CONCLUSIONS

Over the range of heat fluxes considered here the spray evaporative cooling mechanism appears to be that of conduction controlled heat transfer through the droplet with evaporation only at the droplet surface. The question of whether boiling within a droplet ever begins before the Leidenfrost state temperature, T_v , is reached is a very important one which is left unanswered here due to the limited range considered.

The effect of lowering the surrounding pressure is quite marked. Apparently as a result of the decreased "wettability" (increased ϕ) of the liquid on the aluminum surface the flooding coefficient h^* decreases and the Leidenfrost state temperature $T_v - T_s$ increases resulting in $q_m^* = h^* (T_v - T_s)$ remaining essentially constant.

Spray film cooling at atmospheric pressure appears to be relatively independent of any parameters other than the fluid-surface pair. The spray film cooling heat transfer at vacuum pressures appears to be one of conduction through the liquid film with no nucleate boiling within the liquid film ever observed. The liquid film thickness appears to be a very important parameter at these vacuum pressures.

APPENDIX A: ANALYTICAL ANALYSIS

A. Introduction

From the Experimental Analysis it was hypothesized that a very simple droplet conduction and surface evaporation model would adequately describe the heat transfer mechanism during spray evaporative cooling. Towards this end an evaporative model is developed and compared with the experimental results.

B. Previous Research Efforts

Saburo Toda⁽²²⁾ presents a very simplified analysis for the evaporation time of a liquid film formed from a droplet. He arrives at various relations for the different states of heat transfer that he defines - the evaporative, transitional and film state.

The most significant shortcoming in Toda's analysis is that it assumes droplet impact with a solid surface, whereas his experimental measurements were definitely in the "flooded state". He describes runoff from the surface and shows the same in photographs.

His problem, then, was certainly the case of spray film cooling and should be analyzed as such. The excellent agreement of his analytical analysis with his experimental results appears to be a result of having used his experimental data to evaluate four undetermined constants in the analytical analysis. This appears to be a form of having curve-fitted the analytically developed relationship to the measured experimental data.

Wen-Jei Yang⁽²⁰⁾ develops the equations to be solved to determine the evaporation time for a drop on a solid surface. His hemispherical shape assumption might not be valid for a droplet (less than 1 mm). He does not solve these equations. His main result is that he determines

by an order of magnitude argument that the thermal properties of the surface are not important for $\frac{K}{K_m} \ll 1$, a topic to be considered here shortly.

C. General Analysis

An analysis of droplet evaporation on a dry surface will now be presented with the aim of determining the flooding temperature for each impinging spray mass flux, as was done in the previous experimental procedure. An overall analysis is considered in this section. The specific problem of determining the time to evaporate a single droplet is considered in the following section.

During Toda's research⁽²²⁾ he performed an immensely useful experiment. He dropped single droplets of water of known diameter onto a flat glass plate and measured the "spread diameter", D . From this he determined the average thickness b , using conservation of mass.

A glass-water interface may be quite different than an aluminum-water interface and Toda's droplets were somewhat larger than those considered here, but his data is all that is available at the present. His relation for water at 25°C was

$$b = Cd^m$$

where $m = 0.6$ and $C = 2$ for $b, d \ll \mu\text{m}$.

Consistent with Toda's measurements and visual observations here, a droplet resting on a flat surface may be modeled as a thin, right circular cylinder of liquid. This greatly simplifies the formulation and solution of the analytical model.

Consider the droplet of Figure 19. At the onset of flooding, as soon as this droplet evaporates another arrives to replace it. The heat

transfer at this point is then found by considering a single droplet evaporation as:

$$q^* = \frac{(\text{total energy transferred})}{(\text{total time})(\text{average area})} \quad (\text{A.1})$$

where

$$\text{total energy transferred} = \rho \lambda^* b_o A_o \quad (\text{A.2})$$

where:

$$A_o = \frac{\pi}{4} D_o^2 \quad (\text{A.3})$$

$$\text{total time} = \tau_t \quad (\text{A.4})$$

(to be determined in the following section)

$$\text{average area} = A_t \quad (\text{A.5})$$

A droplet will contract at the edges as it evaporates such that the average area will be less than the original area, A_o . The average droplet area will be determined from the average "spread diameter", \bar{D} , as:

$$\bar{A} = \frac{\pi}{4} \bar{D}^2 \quad (\text{A.6})$$

Introducing an "area reduction factor", A_x :

$$\bar{A} = A_x A_o \quad (\text{A.7})$$

then

$$A_x = \left[\frac{\bar{D}}{D_o} \right]^2 \quad (\text{A.8})$$

A_x will be determined in the following section.

Assuming a square lattice of droplets upon the surface, the proportion of the surface area covered by evaporating droplets will be:

$$\frac{\bar{A}}{A_t} = \frac{A_{\text{circle}}}{A_{\text{square}}} = \frac{\frac{\pi}{4} \bar{D}^2}{\bar{D}^2} = \frac{\pi}{4} \quad (\text{A.9})$$

then, using Eq. (A.7):

$$A_t = \frac{4}{\pi} A_x A_o \quad (\text{A.10})$$

Substituting Equations (A.2), (A.4), and (A.10) into Equation (A.1):

$$q^* = \frac{\pi}{4} \frac{\rho \lambda^* b_o}{\tau_t A_x} \quad (\text{A.11})$$

where τ_t and A_x will be evaluated in the following section.

D. Time to Evaporate a Single Droplet

The next major assumption must now be made. Assume that the thermal properties of the surface (conductivity and specific heat) are unimportant for most applications.

As stated previously, Yang⁽²⁰⁾ found this to be the case generally for $K/K_m \ll 1$. In Appendix B this is determined by a much more simplified model, appropriate only for order of magnitude arguments.

One might turn to other research fields to support this assumption. In the case of drop-wise condensation the same question has arisen. However, the two most recent investigations in the subject (53,54,55) find the surface thermal properties to be of significant importance and of no importance respectively. Both experiments were performed with exceptional care. Nonetheless, for the present case the surface temperature may be assumed to remain constant throughout the droplet evaporation.

Referring to Figures 19 and 20, the solution must be broken into two domains:

- 1) Adiabatic Boundary. This domain lasts until the surface temperature of the droplet is raised to the saturation temperature.
- 2) Moving phase front boundary. After the droplet surface is raised to T_s all heat transferred to the surface will act to evaporate mass at the surface. This domain lasts until the thickness decreases to zero.

1) First domain:

This is a classical problem given in several references. Carslaw and Jaeger give the exact solution (56):

$$\begin{aligned} \frac{T - T_o}{T_w - T_o} = \sum_{n=0}^{\infty} (-1)^n \operatorname{erfc} \left[\frac{(2n+1)b_o - x}{\sqrt{2} \sqrt{k\tau}} \right] \\ + (-1)^n \operatorname{erfc} \left[\frac{(2n+1)b_o + x}{\sqrt{2} \sqrt{k\tau}} \right] \end{aligned} \quad (\text{A.12})$$

To solve the inverse problem here of finding $\tau = \tau_1$ when $T = T_s$, it is easiest to use the charts provided in this reference.

2) Second domain:

An approximate integral solution will be employed here (57).

Define $t = \tau - \tau_1$

The governing equation is:

$$\frac{\partial}{\partial t} \int_0^{b(t)} \theta(x) dx + \alpha \left. \frac{\partial \theta}{\partial x} \right|_{x=0} - \alpha \left. \frac{\partial \theta}{\partial x} \right|_{x=b(t)} = 0 \quad (\text{A.13})$$

where $\theta = T - T_s$ measures the internal energy of the volume relative to T_s , simplifying the boundary conditions and allowing consideration of

only the latent heat energy which crosses the outer liquid surface.

In Appendix C it is shown that an energy balance at the surface will yield:

$$\rho \lambda n \frac{db}{dt} = k \left. \frac{\partial \theta}{\partial x} \right|_{x=b(t)} \quad (\text{A.14})$$

where $n = 3/m$.

A parabolic profile will satisfy all of the boundary conditions:

$$\theta(0) = 1$$

$$\theta(b, t) = 0$$

$$\left. \frac{\partial \theta}{\partial x} \right|_{x=b(t)} = \frac{\rho \lambda n}{k} \frac{db(t)}{dt} = s(t)$$

Hence, assume:

$$\theta(x, t) = \theta_w - \left(s(t) + \frac{2\theta_w}{b(t)} \right) x + \left(\frac{s(t)b(t) + \theta_w}{b^2(t)} \right) x^2 \quad (\text{A.15})$$

Now, evaluating each term in Eq. (A.13) yields:

$$\frac{\partial}{\partial t} \int_0^{b(t)} \theta(x) dx = \frac{\theta_w}{3} b' - \frac{\rho \lambda n}{6k} [2bb'^2 + b^2 b''] \quad (\text{A.16})$$

$$\alpha \left. \frac{\partial \theta}{\partial x} \right|_{x=0} = -\alpha \left[s(t) + \frac{2\theta_w}{b(t)} \right] \quad (\text{A.17})$$

$$\alpha \left. \frac{\partial \theta}{\partial x} \right|_{x=b(t)} = \alpha s(t) \quad (\text{A.18})$$

where

$$\alpha = \frac{k}{\rho C_p} \quad (\text{A.18})$$

$$b' = \frac{db}{dt}$$

$$b'' = \frac{d^2b}{dt^2}$$

Substituting these results into Eq. (A.13) and combining terms gives:

$$b'' = - \left[\frac{2}{b(t)} (b')^2 + (12\alpha - \frac{2k\theta w}{\rho n \lambda}) \frac{b'}{b^2} + \frac{12\alpha k}{\rho n \lambda} \frac{\theta w}{b^3} \right] \quad (A.19)$$

with the initial conditions:

$$b(0) = b_0 \quad (A.20)$$

$$b'(0) = 0 \quad (A.21)$$

The second condition matches the 1st and 2nd domains by specifying an adiabatic boundary at the beginning of the second domain.

A solution to Eq. (A.19) was attempted on a digital computer using the very simple Euler integration technique. Unfortunately, this algorithm would become unstable as $b(t) \rightarrow 0$. Decreasing the step size would not eliminate the instability, but only increase the time before it began.

To obtain an approximate closed form solution the higher order term b'' may be eliminated. Solving the resulting quadratic equation for b' , separating variables and integrating (using $b(0) = b_0$) yields:

$$t = \frac{2(b_0^2 - b^2)}{a \pm [a^2 - 8c]^{\frac{1}{2}}} \quad (A.22)$$

where

$$a = 12\alpha - \frac{2k\theta w}{\rho n \lambda}$$

$$c = 12 \frac{\alpha k \theta w}{\rho n \lambda}$$

A difficulty arises in choosing the \pm sign above. There is little

foresight which may be employed here. Yet another approximate closed form solution of (A.19) is obtained if both b'' and $(b')^2$ are eliminated. The resulting approximate solution is

$$b^2(t) = b_o^2 - 12 \alpha \left[\frac{6n\lambda}{C_p \theta_w} - 1 \right]^{-1} \quad (\text{A.23})$$

from which

$$\tau_2 = \frac{b_o^2}{12\alpha} \left[\frac{6n\lambda}{C_p \theta_w} - 1 \right] \quad (\text{A.24})$$

3) Calculating τ_t and A_x :

$$\text{By definition } \tau_t = \tau_1 + \tau_2 \quad (\text{A.25})$$

From Eq. (A.8)

$$A_x = \left[\frac{\bar{D}}{D_o} \right]^2$$

by definition

$$\bar{D}^2 = \frac{1}{\tau_t} \int_0^{\tau_t} D^2(t) dt \quad (\text{A.26})$$

In Appendix C (Eq.C.5) it is shown that:

$$D(t) \sim b^p(t) \quad \text{where} \quad p = \frac{1}{2} \left(\frac{3}{m} - 1 \right)$$

Substituting

$$A_x = \frac{\bar{D}^2}{D_o^2} = \frac{1}{\tau_t b_o^{2p}} \int_0^{\tau_t} b^{2p}(t) dt \quad (\text{A.27})$$

Upon noting that for $0 < \tau < \tau_1$ $b(t) = b_o$

$$A_x = \frac{1}{\tau_t b_o^{2p}} \left[\tau_1 b_o^{2p} + \int_0^{\tau_2} b^{2p}(t) dt \right] \quad (\text{A.28})$$

Substituting Eq. (A.23)

$$\int_0^{\tau_2} b^{2p}(t) dt = \frac{C_1 b_o^{2(p+1)}}{12\alpha (p+1)} \quad (\text{A.29})$$

then

$$A_x = \frac{\tau_1}{\tau_t} + \frac{C_1 b_o^2}{12\alpha (p+1) \tau_t} \quad (\text{A.30})$$

From Eq. (A.24)

$$\frac{C_1 b_o^2}{12\alpha} = \tau_2 \quad (\text{A.31})$$

then

$$A_x = \frac{1}{\tau_t} \left[\tau_1 + \frac{\tau_2}{(p+1)} \right] \quad (\text{A.32})$$

for the case $\tau_1 \ll \tau_2$

$$A_x = \frac{1}{(p+1)} \quad (\text{A.33})$$

E. Total solution

Upon substituting τ_t and A_x determined in the previous section (Eq. [A.25] and Eq. [A.32]) into Eq. (A.11) of Section C:

$$q^* = \frac{\pi}{4} \rho \lambda^* b_o \left[\tau_1 + \frac{\tau_2}{p+1} \right]^{-1} \quad (\text{A.34})$$

where

$$p = \frac{1}{2} \left(\frac{3}{m} - 1 \right)$$

$$\tau_1 = \text{found in ref. 56}$$

$$\tau_2 = \frac{b_o^2}{12\alpha} \left[\frac{6(1+2p)\lambda}{C_p \theta_w} - 1 \right]$$

The assumptions implicit in this solution are:

- one-dimensional conductive heat transfer through a thin right cylinder of fluid with evaporation at the surface only

- the average thickness is related to the initial droplet diameter through a power law, i.e. $b \sim d^m$.
- the higher order terms b'' and $(b')^2$ in Eq. (A.19) may be neglected.

A much simpler relation may be obtained if two approximations are made.

For the present case take:

$$\tau_2 \gg \tau_1 \quad (2\% \text{ max. error})$$

and

$$\frac{6}{C_p} \frac{(1+2p)\lambda}{\theta_w} \gg 1 \quad (0.2\% \text{ max. error})$$

Using the definition of h^* (Eq. [4]), Eq. (A.34) reduces to:

$$h^* = \frac{\pi}{2} \frac{K}{b_o} \left(\frac{\lambda^*}{\lambda} \right) \left[\frac{p+1}{2p+1} \right] \quad (\text{A.36})$$

It is very interesting to note that all dependence upon ρC_p cancels out as a result of the two opposing effects it has upon the heat transfer rate (increasing the evaporation time but increasing the heat transferred to a droplet by the same proportion). λ has a very small effect upon h^* . For spray fluid which is not subcooled it has no effect at all. The dependence upon p is equally small, the term depending upon p can vary only from 1 at $p = 0$ to $1/2$ at $p = \infty$.

The similarity between Eq. (A.36) and a steady liquid film conduction model is equally interesting. Taking a time average droplet thickness of $1/2 b_o$ would yield Eq. (A.36) minus the λ , λ^* , and terms.

These interesting results may be a result of having neglected

the higher order terms in Eq. (A.19)

From Toda's droplet measurements ⁽²²⁾, with $\bar{d}_v = 155\mu\text{m}$, $b_o = 41\mu\text{m}$. Equation (A.36) may be evaluated for three different assumptions concerning p :

- a) A simplified model might have taken $n = 1$ (or $p = 0$) in Eq. (A.14) and $A_x = 1$ in Eq. (A.7). For this case:

$$h^* = 29.9 \text{ Kw/m}^2\text{-}^\circ\text{C}$$

- b) In the absence of Toda's ⁽²²⁾ measurements an assumption that all droplets have the same shape would seem reasonable. This implies $p = 1$ from which:

$$h^* = 20.0 \text{ Kw/m}^2\text{-}^\circ\text{C}$$

- c) For the purposes here, Toda's ⁽²²⁾ experimentally determined value $m=0.6$ (or $p=2$) will be used. This yields:

$$h^* = 18.0 \text{ Kw/m}^2\text{-}^\circ\text{C}$$

The experimental analysis determined

$$h^* = 15.4 \pm 3 \text{ Kw/m}^2\text{-}^\circ\text{C}$$

As might be expected, assumption (c) predicts most accurately this experimentally determined value.

The most fruitful additions to this analytical model should result from two improvements - (1) an exact numerical solution of Eq. (A.19) and (2) improved measurements of the droplet spread diameter as a function of the initial spherical diameter for distilled water upon an aluminum surface. Including internal convection within a droplet or considering the droplet surface shape to be curved as opposed to the planar, average thickness used here would only increase

the difference between the analytical and experimental results.

APPENDIX B: ANALYSIS OF SURFACE CONDUCTIVITY EFFECTS

The goal here is to determine whether the thermal properties of the surface upon which a droplet evaporates will significantly affect the evaporation process. The "worst possible" case will be considered; that of allowing a single droplet to strike a dry surface at a temperature above the liquid saturation temperature. For convenience, a hemispherical droplet shape will be assumed.

The effort is simply an order of magnitude argument. For this reason, a very simplified analytical solution to the above problem will be quite satisfactory.

During the "quasi-steady" evaporation of the droplet, after the initial instantaneous transients have died out and the droplet surface is at temperature T_s , the problem may be modeled as shown in Figure 18. All of the energy is assumed to cross the liquid-metal interface through a spherical lumped volume ($k = \infty$) of diameter $\frac{1}{2}d$ and at a temperature T_w . Heat is conducted in from infinity within the surface metal, and outward to the droplet surface through the liquid.

The thermal resistances are found as:

$$R = \frac{1}{2\pi k} \int_{r_1}^{r_2} \frac{dr}{r^2} \quad (B.1)$$

$$\text{so that : } R_{\ell} = \frac{1}{\pi d k} \quad (B.2)$$

$$R_{\infty} = \frac{2}{\pi d k_m} \quad (B.3)$$

$$\text{Then, } \frac{R_{\infty}}{R_{\ell}} = 2 \frac{K}{K_m} \quad (B.4)$$

Hence, as found by Yang (20), for

$$\frac{K}{K_m} \ll 1 \quad (B.5)$$

the thermal properties of the surface are unimportant.

If thermal capacitances are included in the analysis, the result is more emphatic. In the metal, they would effectively lower the thermal resistance by supplying an energy source closer than that at infinity. Whereas, in the liquid, they would effectively raise the thermal resistance by providing an inertial heat sink that must be filled in addition to the heat conducted to the liquid surface.

For the water - aluminum case considered here :

$$\frac{K}{K_m} = 8.6 \cdot 10^{-3} \ll 1 \quad (B.6)$$

For liquid metals ($K \approx 50 \text{ Btu/hr} \cdot \text{ft} \cdot ^\circ\text{F}$) this would not be the case.

APPENDIX C: ENERGY BALANCE AT THE DROPLET SURFACE

If the evaporation at the liquid surface caused only a one-dimensional change in the average droplet thickness, an energy balance would yield:

$$K \frac{dT}{dx} \bigg|_{x=b(t)} = p \lambda \frac{d\hat{b}}{dt} \quad (C.1)$$

where $\hat{b}(t)$ would be the resulting one-dimensional height.

However, as mass is evaporated at the surface, the edges of the droplet would move inward to maintain ϕ constant.

Figure 21 (a) depicts the initial droplet shape for a right circular cylinder model. Figure 21 (b) shows the result of a one-dimensional change. Figure 21 (c) depicts the final configuration after the edges move inward.

Conservation of mass yields:

$$\frac{\pi}{4} D^2 \hat{b} = \frac{\pi}{4} \tilde{D}^2 \tilde{b} \quad (C.2)$$

An experimental analysis such as Toda's ⁽²²⁾ would determine:

$$b \sim d^m \quad (C.3)$$

However, $b = b(D)$ is what is of interest. Towards this end, conservation of mass gives :

$$\frac{\pi}{4} D^3 = \frac{\pi}{4} b D^2 \quad (C.4)$$

Substitute Eq. (C.3) and rearrange terms:

$$D \sim b^p \quad (C.5)$$

$$\text{where } p = \frac{1}{2} \left(\frac{3}{m} - 1 \right)$$

Then,

$$\tilde{D} = \left(\frac{\tilde{b}}{b}\right)^p D \quad (C.6)$$

Making this substitution into Eq. (C.2):

$$\hat{b} = \frac{\tilde{b}^{(1+2p)}}{b^{2p}} \quad (C.7)$$

Holding b constant for the differentiation and noting that $\tilde{b} \rightarrow b$ in the limit implied by the differentiation:

$$\left. \frac{d\hat{b}}{dt} \right|_{b(t)} = n \frac{db}{dt} \quad (C.8)$$

$$\text{where } n = 1+2p = 3/m$$

Equation (C.1) then becomes:

$$\left. \frac{KdT}{dx} \right|_{x=b(t)} = \rho n \lambda \frac{db}{dt} \quad (A.14)$$

REFERENCES

1. Levitan, L.L. and F.P. Lantsman, "Investigating burnout with flow of a steam-water mixture in a round tube", Thermal Engineering 22, 102 (1975).
2. Parker, J.P. and Grosh, R.J., "Heat transfer to a mist flow", U.S.A.E.C. rep. nr. ANL-6291, (1961).
3. Fikry, M.M., "Heat transfer to wet steam flowing in a horizontal tube", Ph.D. Thesis, Univ. of London, (Oct. 1952).
4. Hiroyasu, H., T. Kadota and T. Senda, "Evaporation of a fuel droplet contacting with a hot surface in a pressurized and heated ambient gas", Trans. JSME, 39(328), 3779 (1973).
5. Tamura, Z. and Y. Tanasawa, "Evaporation and combustion of a drop contacting with a hot surface," 7th Symposium (International) on Combustion, Butterworth's Scientific Publications, London, 509 (1959).
6. Yang, W.-J., "Vaporization and combustion of binary liquid drops on heated surface", Proc. 1977 Tokyo Joint Gas Turbine Congress, 77 (1977).
7. Savic, P. and G.T. Boulton, "The fluid flow associated with the impact of liquid drops with solid surfaces", National Research Council of Canada, rep. nr. MT-26, (May 1955).
8. Bonacina, C. and S. Del Giudice, "Evaporation from cryogenic liquids sprayed on flat surfaces", Proc. 5th Int. Heat Transfer Conf., Tokyo (1974).
9. Mikhaylov, I.F., G.P. Glazunov, and N.A. Kosik, "Evaporation of liquid-nitrogen droplets on metal surfaces," Heat Transfer - Soviet Research, Vol. 7, No. 3, (May-June 1975).
10. Daly, John J. Jr., "Direct contact refrigerant freezing of foods," ASHRAE Journal, (June 1971).
11. Sills, J.T., "Recent advances in the liquid nitrogen freezing of foods," ASHRAE Journal, (June 1971).
12. Dinglinger, G., "Low temperature freezing of food with boiling liquids," Kaltetechnik-Klimatisierung 22, 220-230 (1970).
13. Gallagher, L.V. and B.S. Old, Scientific American (209), 75(1963).
14. Mirua, K., K. Atarashiya, et al., "Experimental study of drying characteristics of single drops containing solids," Heat Transfer - Japanese Research, Vol. 1, No. 2, (April-June 1972).

15. Fisher, Arthur, "What are we going to do about nuclear wastes?", Popular Science, Vol. 213, No. 6, p. 97, (Dec. 1978).
16. Nurick, W.H., J.D. Seader and T.A. Coultas, "Transient heat transfer from a liquid metal spray impinging on a vertical surface," Chemical Engineering Progress Symposium Series, no. 59, 61, p. 127, (1965).
17. Burge, H.L., "High heat flux removal by liquid metal spray cooling of surface," Chemical Engineering Progress Symposium Series, No. 59, 61, p. 115, (1965).
18. Bonacina, C., G. Comini and S. Del Giudice, "Evaporation of atomized liquids on hot surface," Letters in Heat and Mass Transfer Vol. 2, pp. 401-406 (1975).
19. Bonacina, C., G. Comini, and S. Del Giudice, "Evaporazione di liquidi atomizzati a contatto di superfici calde," Quaderni di Fisica Tecnica 58, Padova (1974).
20. Yang, W.-J., "Mechanics of droplet evaporation on heated surfaces," Letters in Heat and Mass Transfer, Vol. 5, pp. 151-166 (1978).
21. Mann, R.F. and W.W. Walker, "The vaporization of small binary drops on a flat plate at maximum heat flux," The Canadian Journal of Chemical Engineering, Vol. 53, (Oct. 1975).
22. Toda, S., "A study of mist cooling - thermal behaviors of liquid film formed from mist drops on a heated surface at high temperatures and high heat fluxes," Tohoku Univ. Technology Reports, Vol. 36, No. 2, (1971).
23. Toda, S. and H. Uchida, "Study of liquid film cooling with evaporation and boiling," Heat Transfer - Japanese Research, Vol. 2, No. 3, (1973).
24. Kopchikov, I.A., G.I. Voronin, et al., "Liquid boiling in a thin film," Int. J. Heat Mass Transfer, Vol. 12, pp. 791-796 (1969).
25. Mesler, R. and G. Allen, "Nucleate boiling in thin films," AIChE Journal, Vol. 23, No. 6, p. 954 (Nov. 1977).
26. Murthy, V.N. and P.K. Sarma, "A note on thin film evaporation - prediction of heat transfer rates," J. Chem. Eng. of Japan, Vol. 6, No. 5, (1973).
27. Hsu, Y.Y., F.F. Simon and J.F. Lad, "Destruction of a thin liquid film flowing over a heated surface," Chem. Eng. Prog. Symposium Ser., No. 57, Vol. 61, p. 139 (1965).

28. Finlay, I.C., "An analysis of heat transfer during flow of an air-water mist across a heated cylinder," The Canadian Journal of Chemical Engineering, Vol. 49, (June 1971).
29. Kosky, P.G., "Heat transfer to a saturated mist flowing normally to a heated cylinder," Int. J. Heat Mass Transfer, 19, 539(1976).
30. Finlay, I.C., "Spray flow as a heat-transfer media", Chemical Processing, 5, pp. 25-29 (1971).
31. Hodgson, J.W. and J.E. Sutherland, "Heat transfer from a spray-cooled isothermal cylinder," Ind. Eng. Chem. Fundls., 7, pp. 567-571, (1968).
32. Leidenfrost, J.G., "De aquae communis nonnullis qualitatibus tractatus," Duisburg (1756) English Translation: Int. J. Heat Mass Transfer, 9, 1153-1166 (Nov. 1966).
33. Bell, K.J., "The Leidenfrost phenomenon: a survey," Chem. Eng. Prog. Symposium Ser., Vol. 63, p. 73 (1967).
34. Gottfried, B.S., C.J. Lee and K.J. Bell, "The Leidenfrost Phenomenon: film boiling of liquid droplets on a flat plate", Int. J. Heat Mass Transfer, Vol. 9, pp. 1167-1187 (1966).
35. Gaugler, Raymond E., "Experimental investigation of spray cooling of high temperature surfaces," Ph.D. Thesis, Carnegie-Mellon University (1966).
36. Schoessow, Glen J., D.R. Jones and K.J. Baumeister, "Leidenfrost film boiling of drops on a moving surface," Chem. Eng. Prog. Symposium Ser., No. 82, 64, p. 95 (1968).
37. Baumeister, K.J. and G.J. Schoessow, "Creeping flow solution of Leidenfrost boiling with a moving surface," Chem. Eng. Prog. Symposium Ser., No. 92, 65, p. 167 (1969).
38. Rao, P.S.V.K. and P.K. Sarma, "Effect of sub-cooling on film boiling heat transfer: droplet evaporation on a hot plate," Journal of Chemical Engineering of Japan, Vol. 7, no. 5, (1974).
39. Hoogendoorn, C.J. and R. den Hord, "Leidenfrost temperature and heat transfer coefficients for water sprays impinging on a hot surface," Proc. 5th Int. Heat Transfer Conf., Tokyo (1974)
40. Emmerson, G.S., "The effect of pressure and surface material on the Leidenfrost point of discrete drops of water", Int. J. Heat Mass Transfer, Vol. 18, pp. 381-386 (1975).
41. Emmerson, G.S. and C.W. Snoek, "The effect of pressure on the Leidenfrost point of discrete drops of water and freon on a brass surface," Int. J. Heat Mass Transfer, Vol. 21, pp. 1081-1086 (1978).

42. Cumo, M., G.E. Farello and G. Ferrari, "Notes on droplet heat transfer," Chem. Eng. Prog. Symposium Ser., No. 92, 65, p. 175 (1969).
43. Wachters, L.H.J., H. Bonne, and H.J. van Nouhvis, "The heat transfer from a hot horizontal plate to sessile water drops in the spheroidal state," Chem. Eng. Sci., Vol. 21, pp. 923-936 (1966).
44. Baumeister, K.J., G.J. Schoessow, and C.E. Chmielewski, "Film boiling of mercury droplets," Can. J. of Chem. Eng., Vol. 55, (Oct. 1977).
45. Hall, W.B., "The stability of Liedenfrost drops," Proc. 5th Int. Heat Transfer Conf., Tokyo (1974).
46. Savic, P., "The cooling of a hot surface by drops boiling in contact with it," National Research Council of Canada, rep. no. MT-37 (April 1958).
47. Monde, M. and Y. Katto, "Burnout in a high heat-flux boiling system with an impinging jet," Int. J. of Heat Mass Transfer, Vol. 21, pp. 295-305 (1978).
48. Aluminum Standards and Data, Aluminum Association, (1970).
49. Alcoa Aluminum Handbook, Aluminum Co. of America, Pittsburgh, Penn., (1956).
50. "Aluminum-properties," Physical Metallurgy, P.D., Kent R. Van Horn, ed., Alcoa, p. 7, (1967).
51. Shero, J.P., "Porous plate sublimator analysis," Ph.D. Thesis, Rice University, Nov. 1969.
52. Zodrow, J., results of summer research, Rice University, Mechanical Engineering Dept., private communication, August 1978.
53. Hannemann, R.J. and B.B. Mikic, "An analysis of the effect of surface thermal conductivity on the rate of heat transfer in dropwise condensation," Int. J. Heat Mass Transfer, Vol. 19, pp. 1299-1307 (1976).
54. Hannemann, R.J. and B.B. Mikic, "An experimental investigation into the effect of surface thermal conductivity on the rate of heat transfer in dropwise condensation," Int. J. Heat Mass Transfer, Vol. 19, pp. 1309-1317 (1976).
55. Rose, J.W., "Effect of condenser tube material on heat transfer during dropwise condensation of steam," Int. J. Heat Mass Transfer, Vol. 21, pp. 835-840 (1978).

56. Carslaw, H.S. and J.C. Jaeger, Conduction of Heat in Solids. Clarendon Press, Oxford, p. 83, (1959).
57. Arpaci, V.S., Conduction Heat Transfer, Addison-Wesley, (1966).

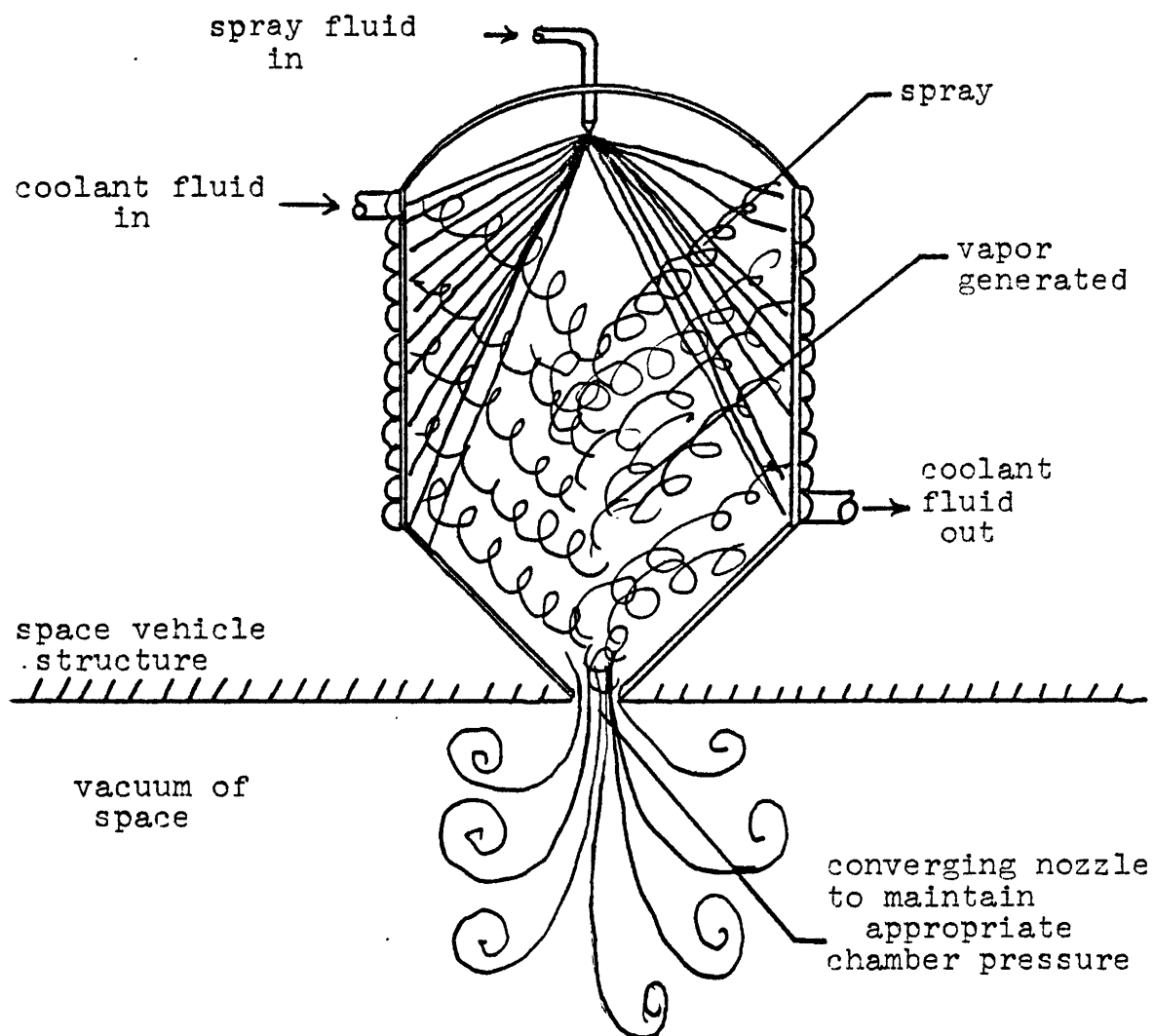


Figure 1. Operation of NASA's "Flash Evaporator System"

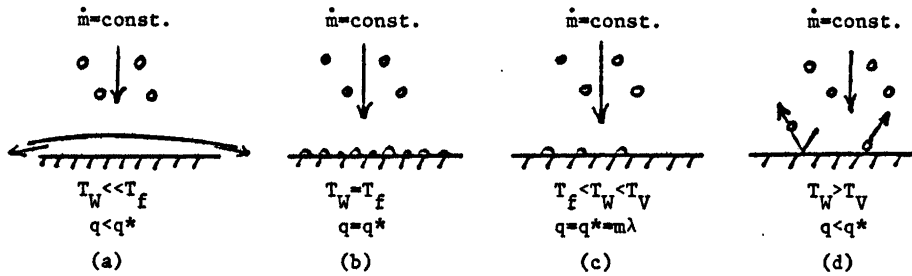


FIGURE 2. The three modes of operation during spray cooling: (a) flooded mode, (c) dry-wall mode, (d) Leidenfrost mode. The transition between (c) and (a) is shown in (b). Figure 3 elaborates upon this transition.

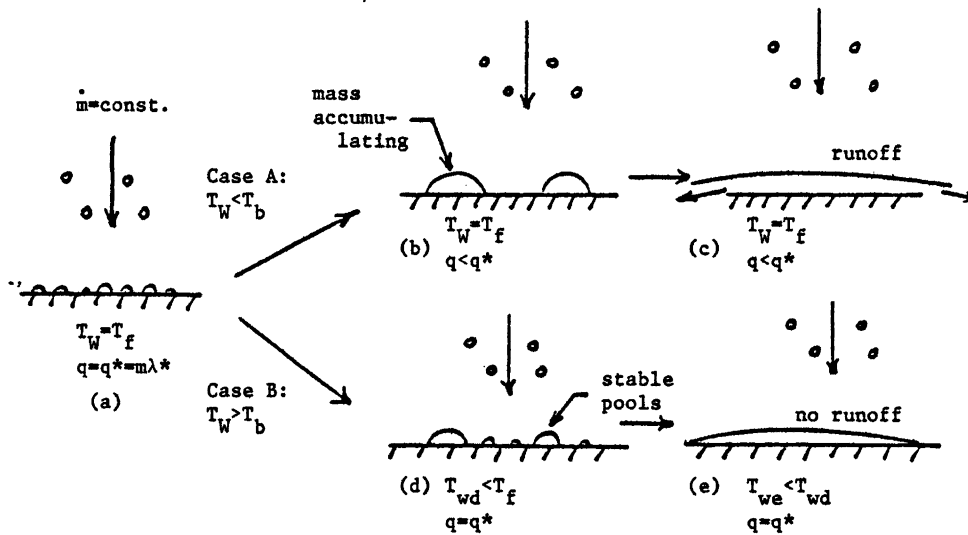


FIGURE 3. Mechanism during transition from dry-wall to flooded modes. For $T_W < T_b$ heat transfer through a pool is less than through a droplet, while for $T_W > T_b$ it is greater.

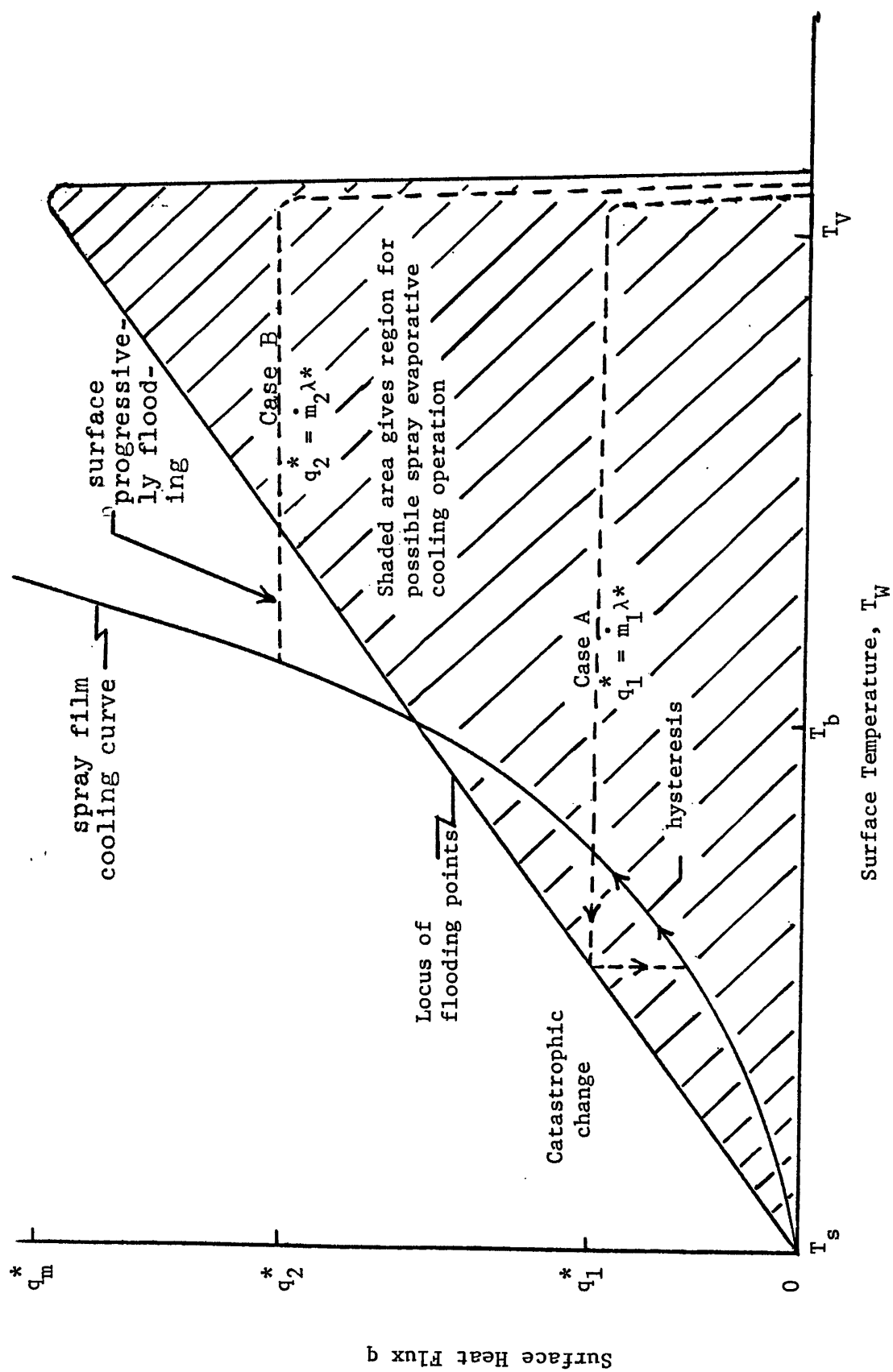


FIGURE 4. Predictions of the "Analysis".

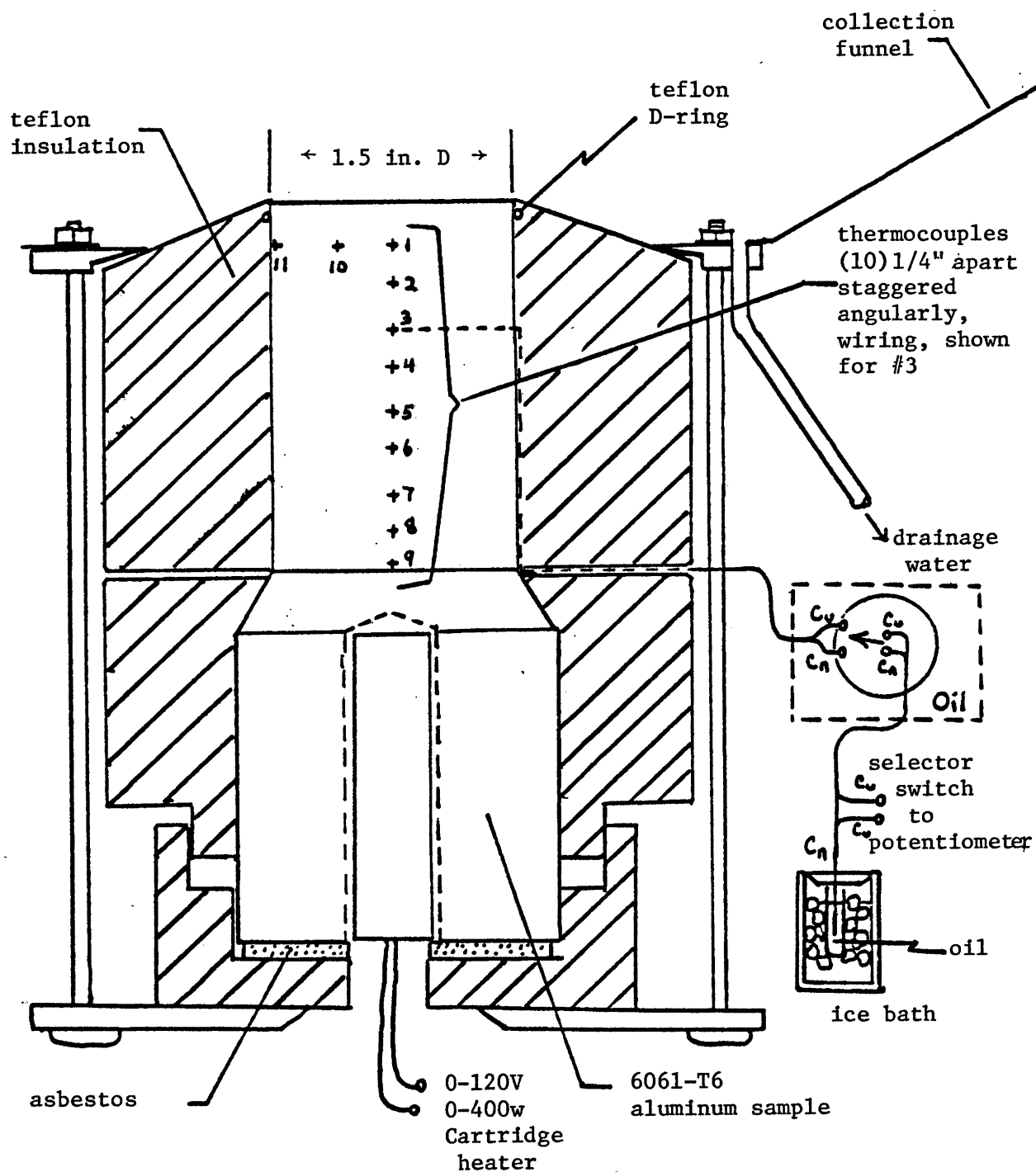


FIGURE 5. Schematic diagram of the heat flux sample.

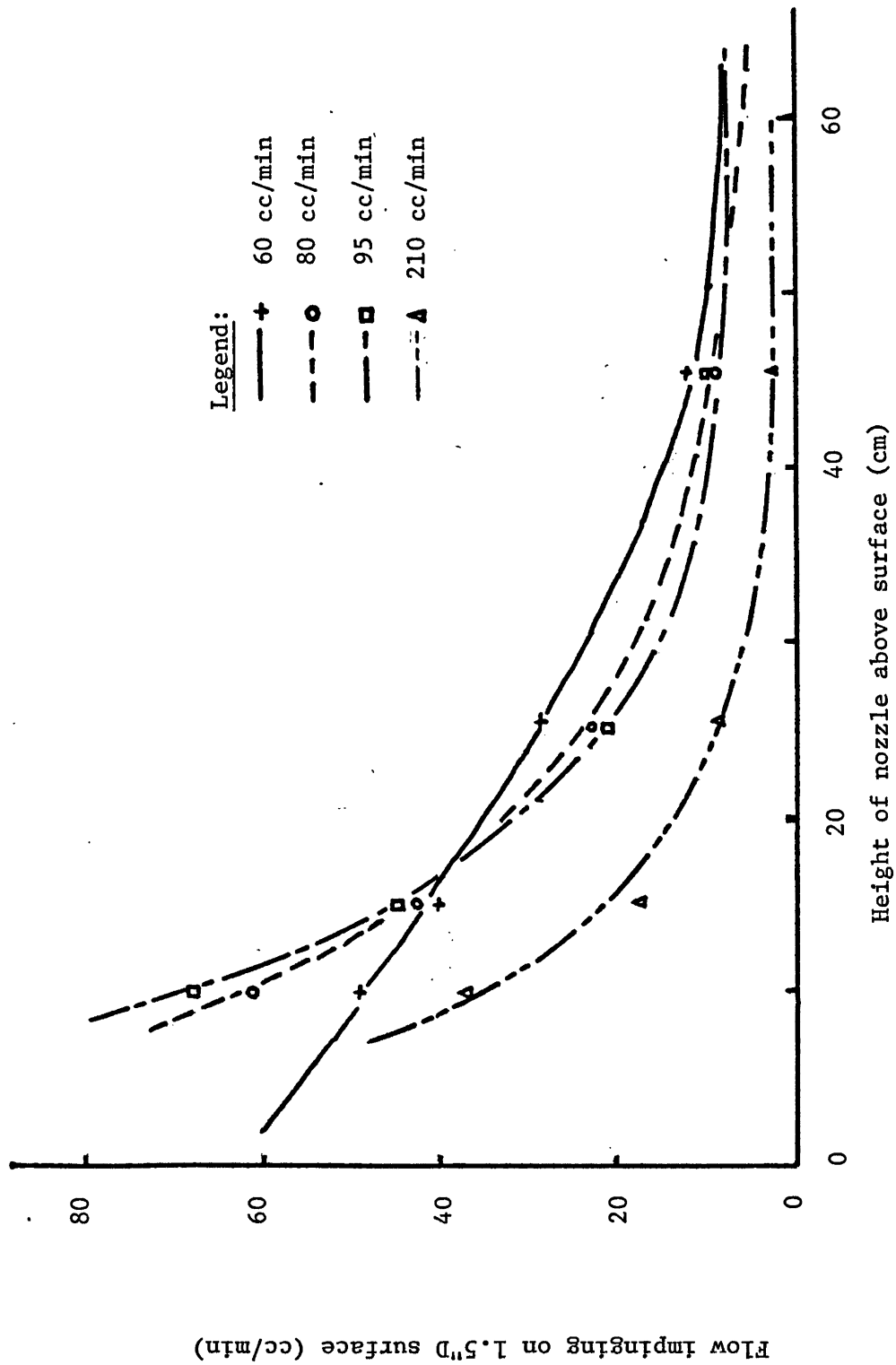
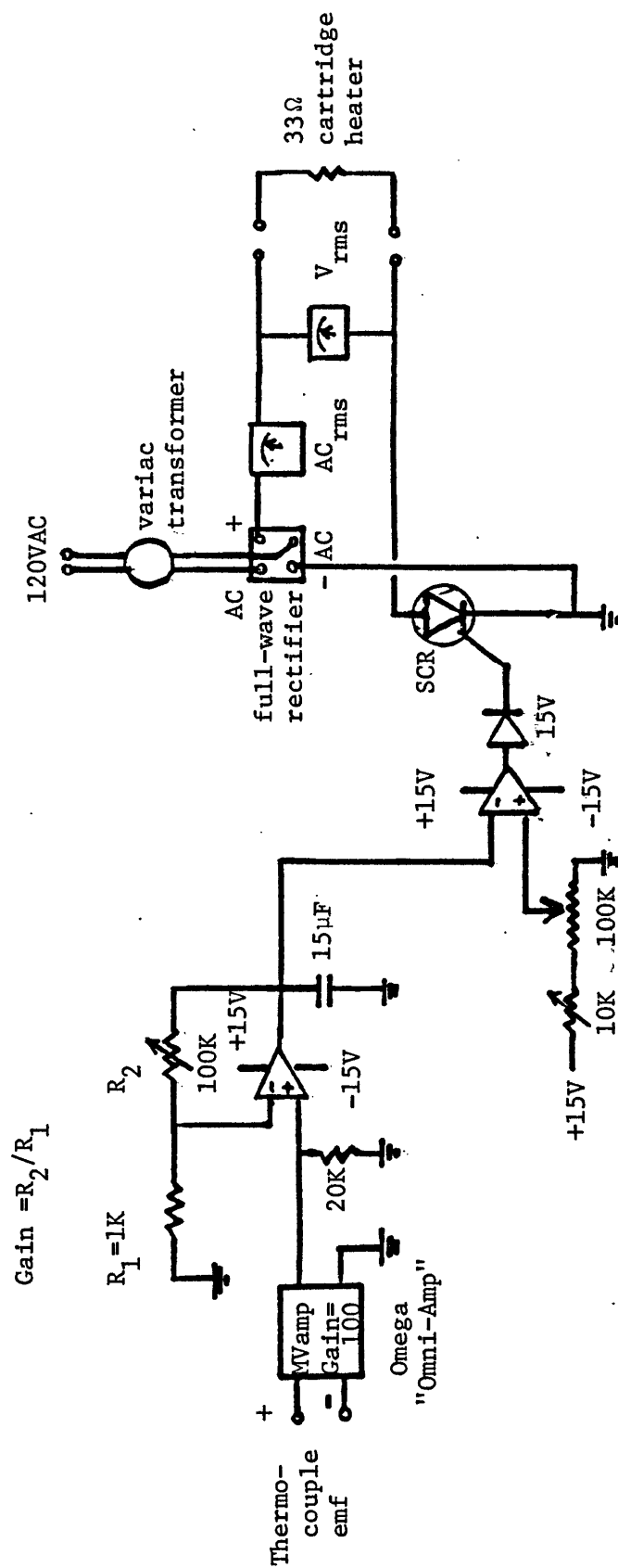


FIGURE 6. Effect of varying spray parameters upon total mass striking surface.



Operational amplifiers - General Electric GEIC-263

FIGURE 7. Original temperature control circuit.

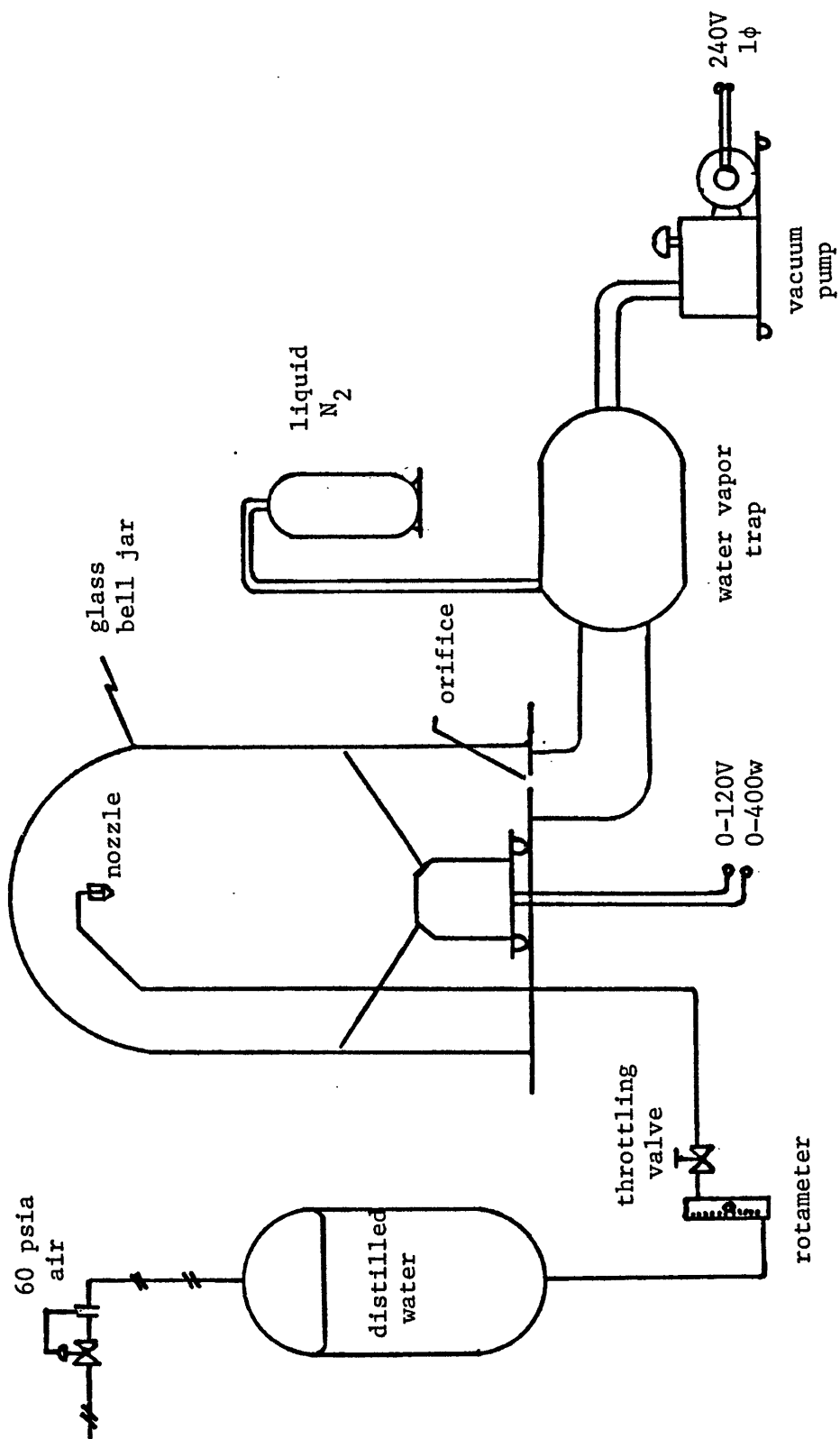


FIGURE 8. Schematic diagram of vacuum system and liquid spray supply.

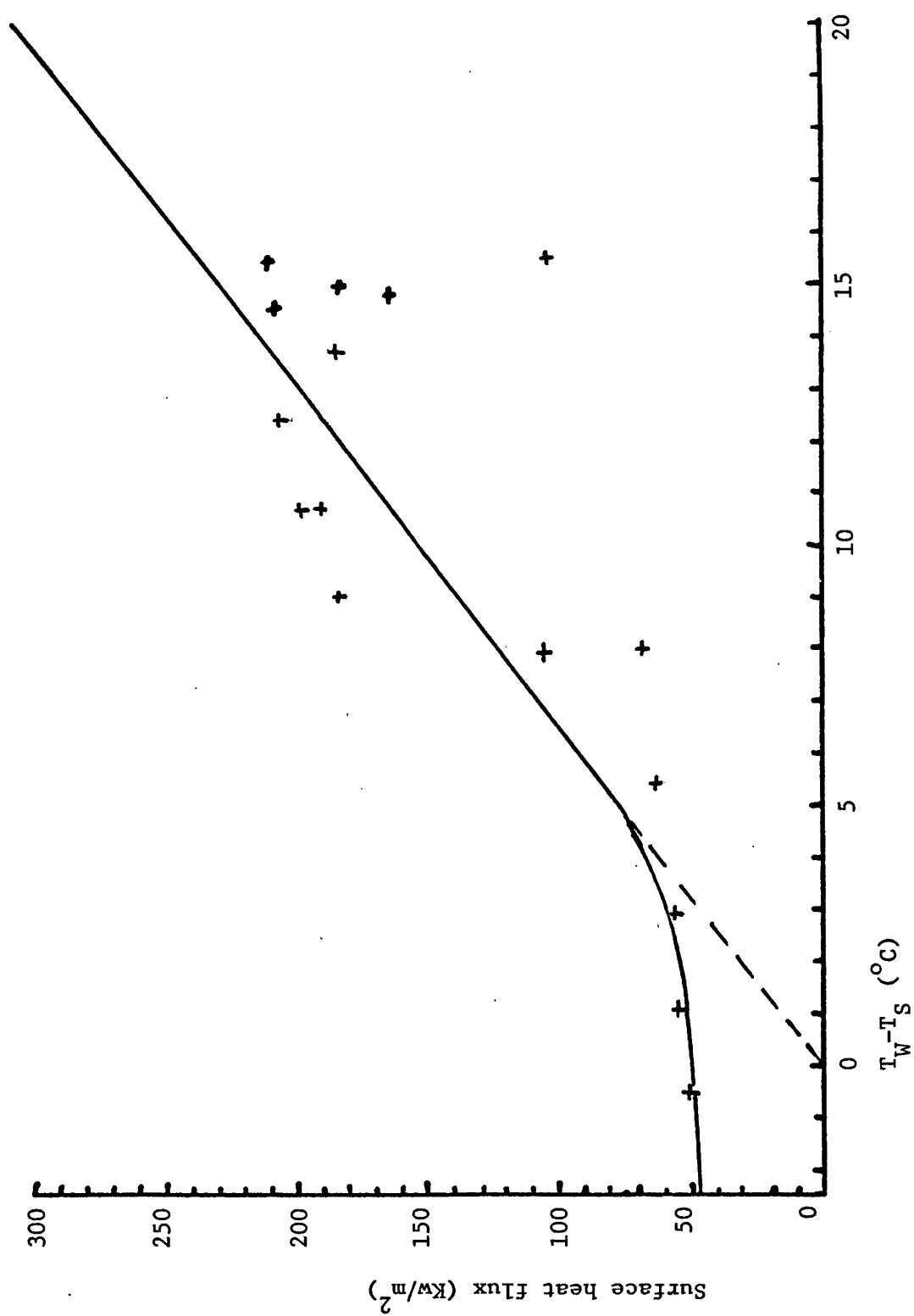


FIGURE 9. Measurements of the flooding locus at atmospheric pressure.

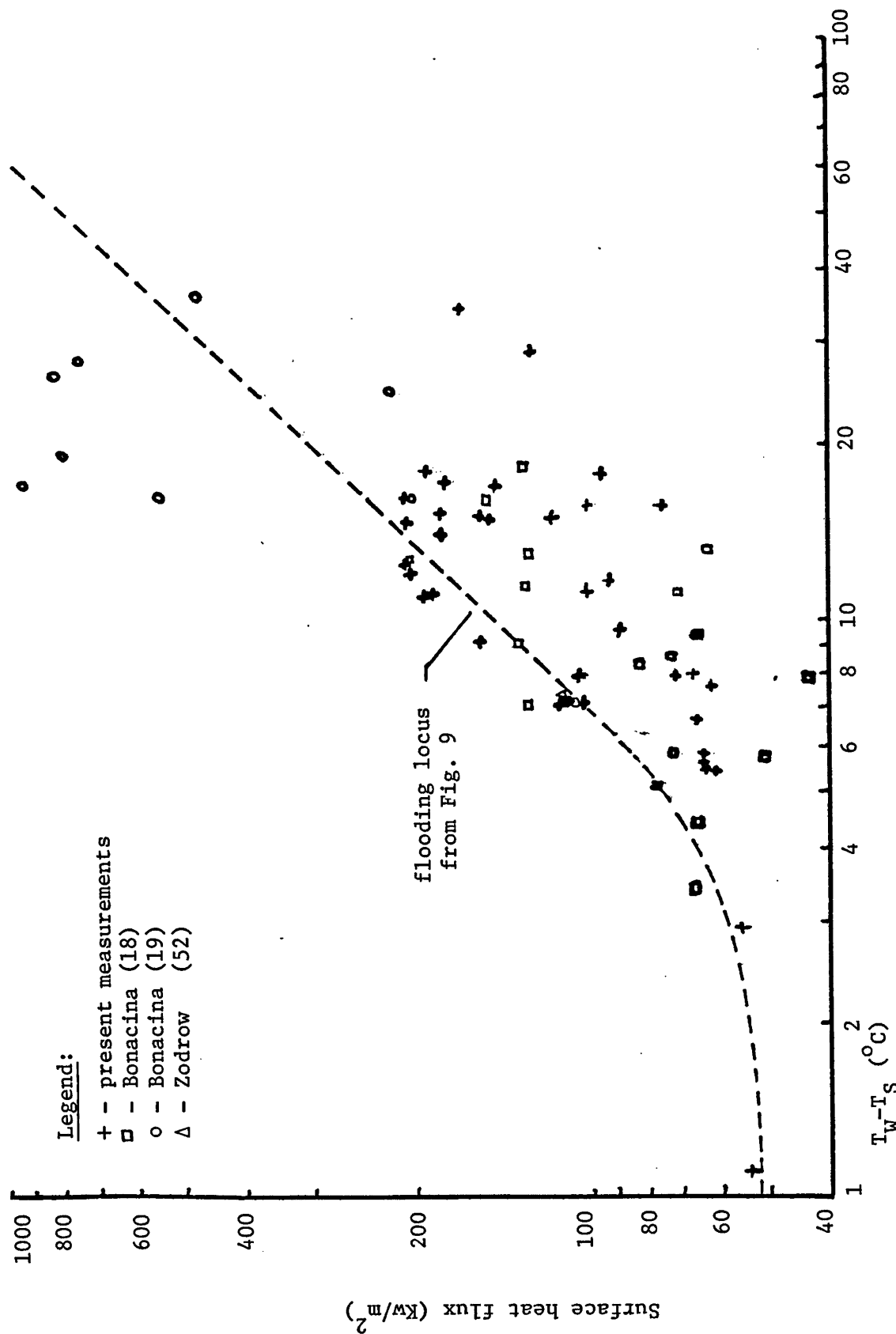


FIGURE 10. Summary of all spray evaporative cooling measurements to date.

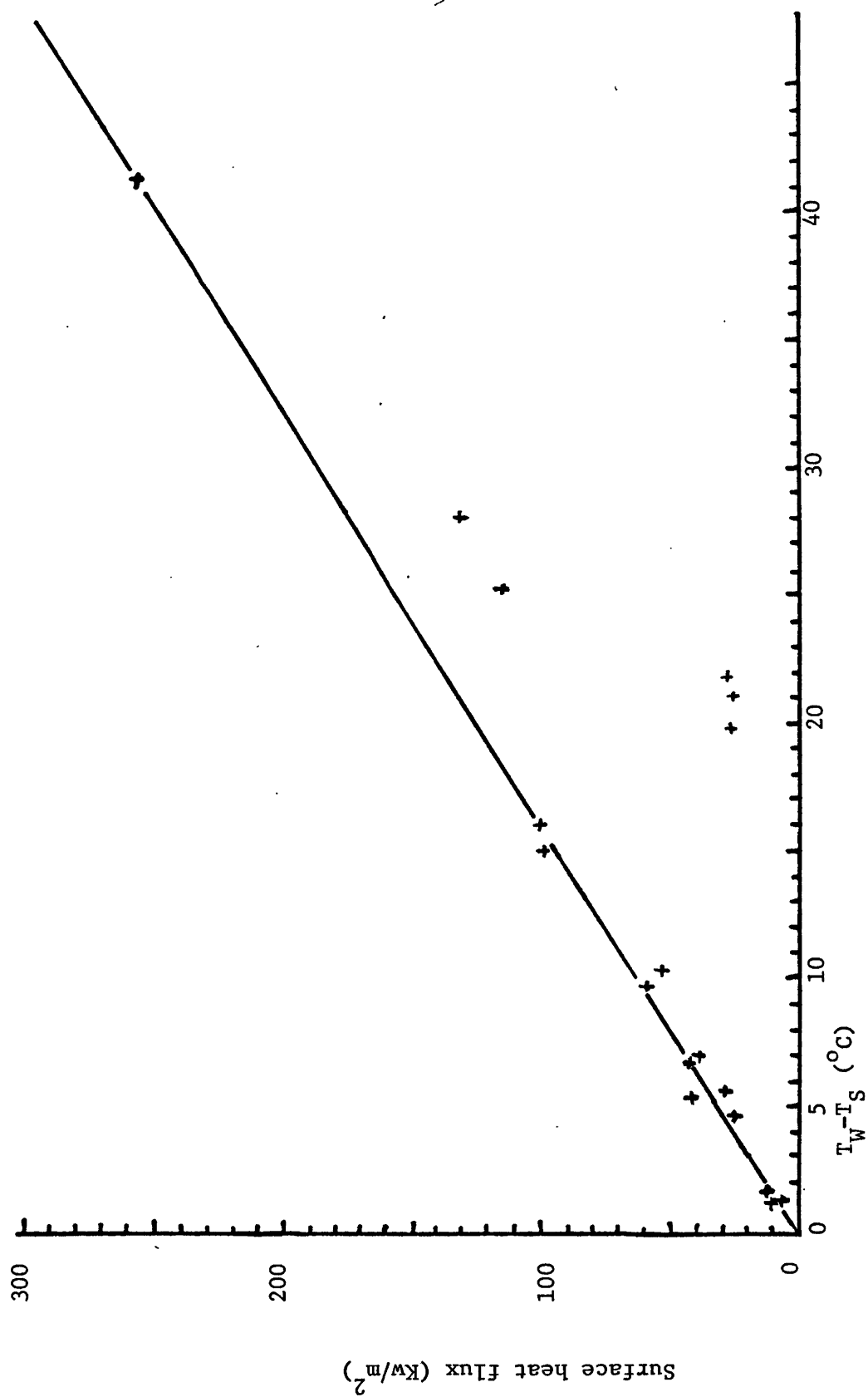


FIGURE 11. Measured flooding locus for $\bar{P}=6.76\text{mmHg}$.

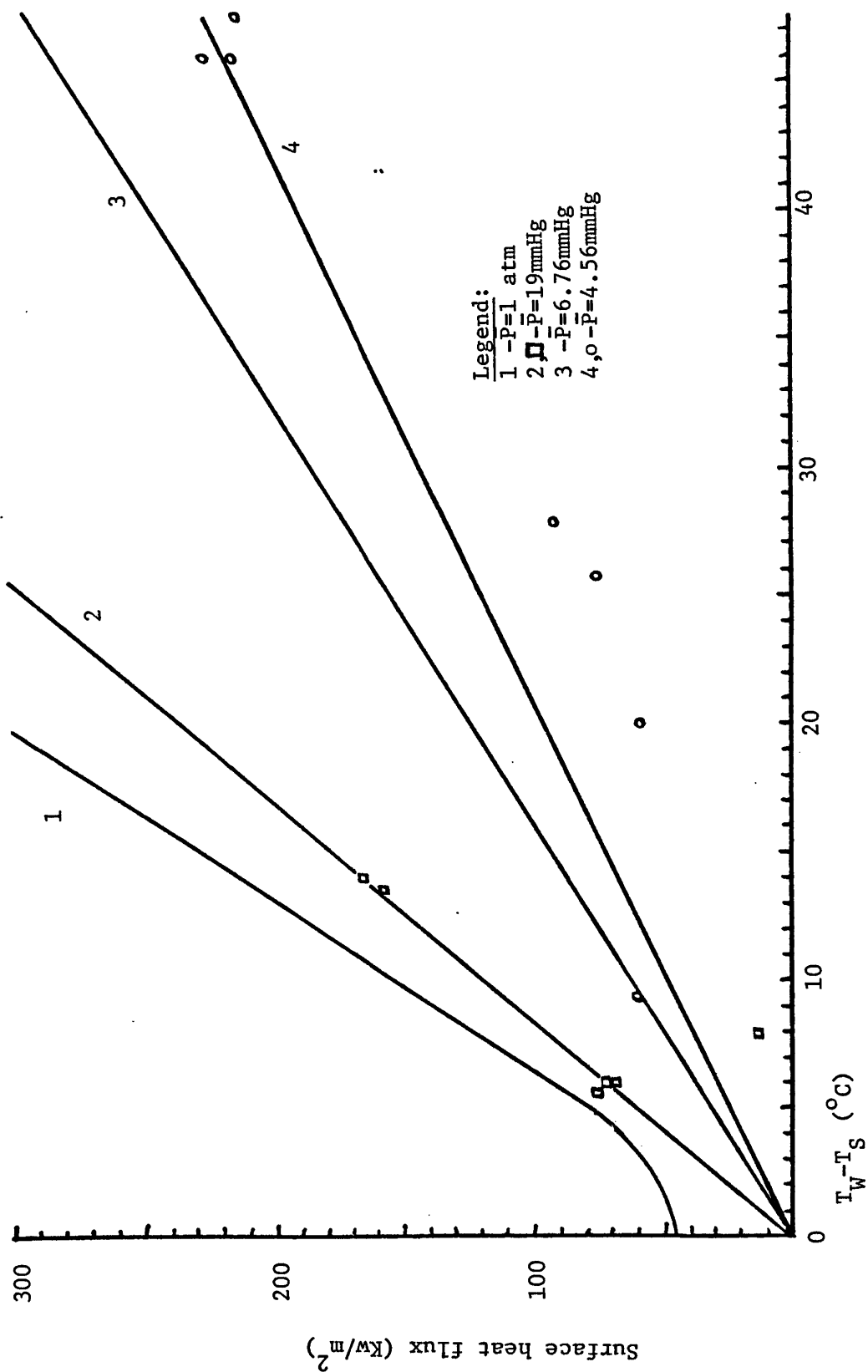


FIGURE 12. The effect of surrounding pressure changes upon the flooding locus.

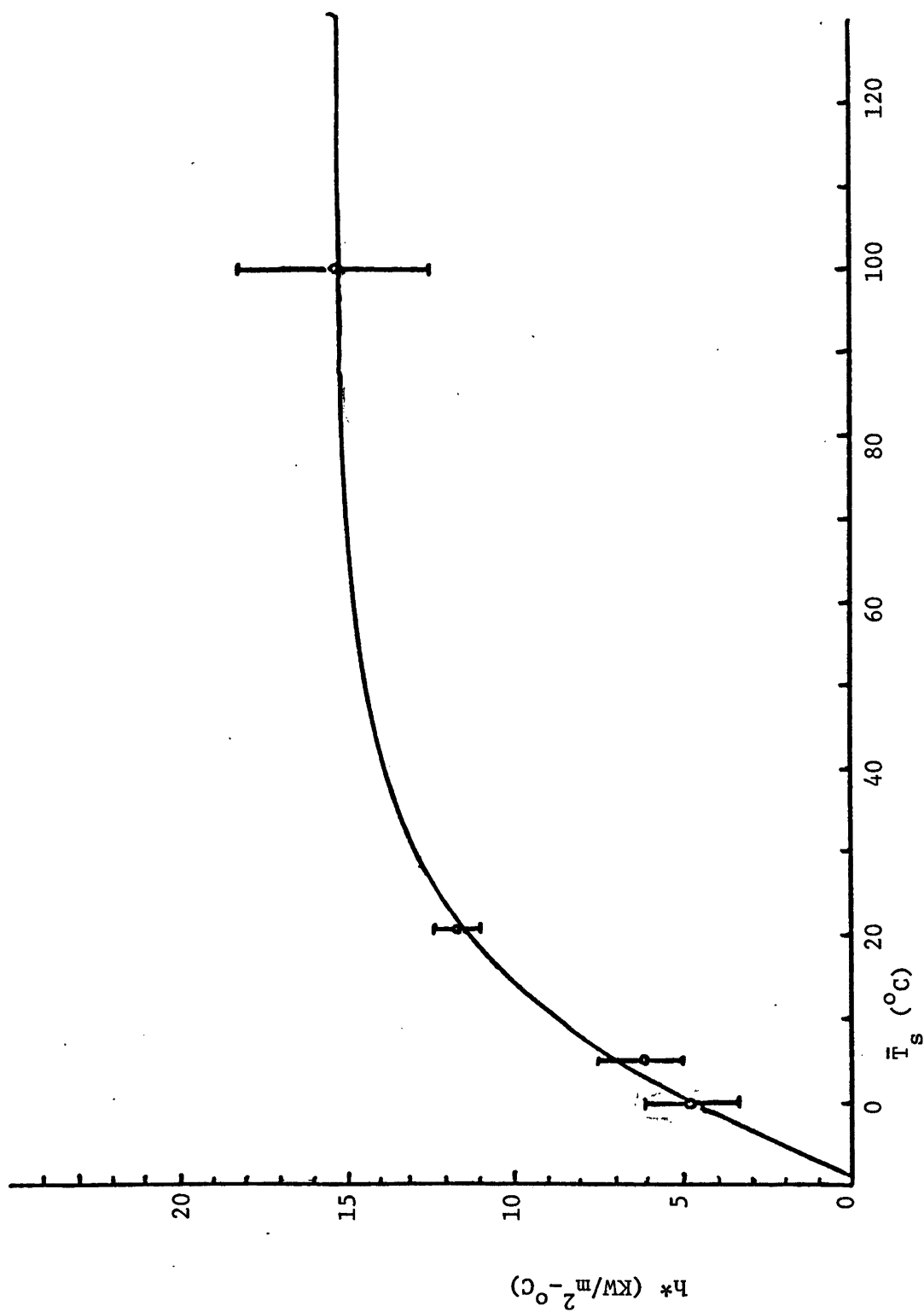


FIGURE 13. h^* as a function of \bar{T}_s .

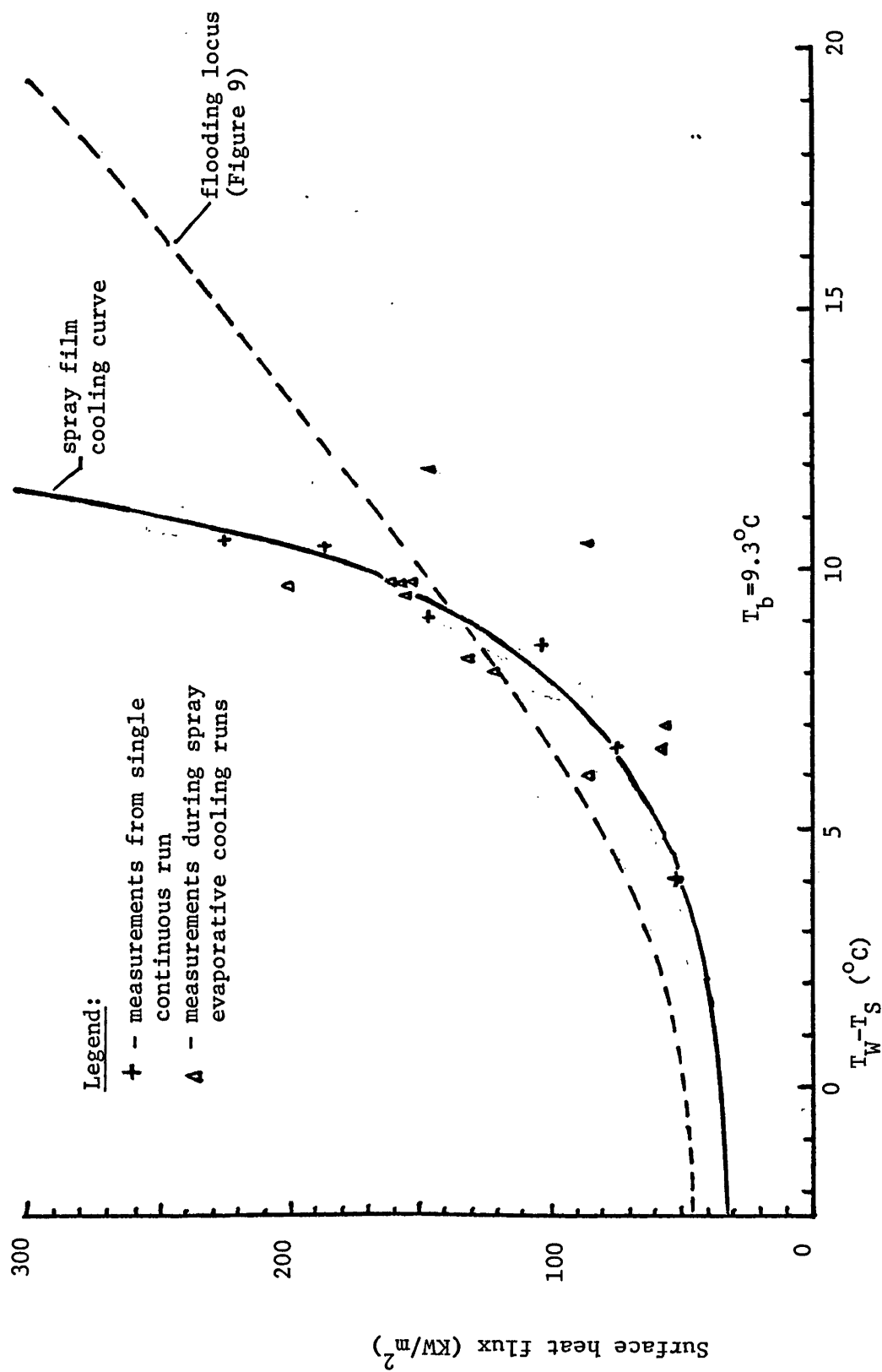


FIGURE 14. Spray film cooling curve compared with flooding curve, atmospheric pressure.

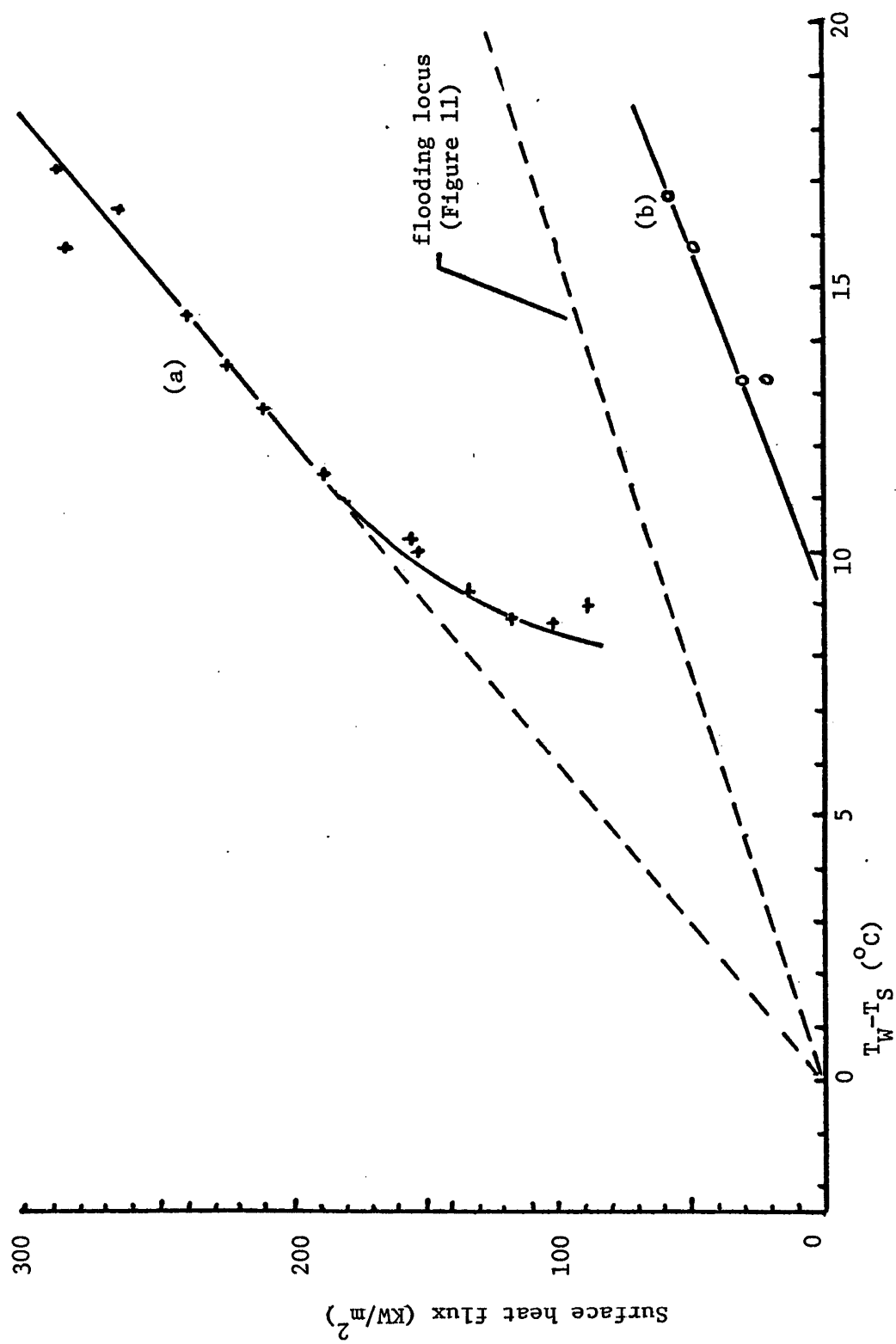


FIGURE 15. Spray film cooling measurements using orifice #2 ($\bar{P}=6.76\text{mmHg}$): (a) thin film (b) thick film.

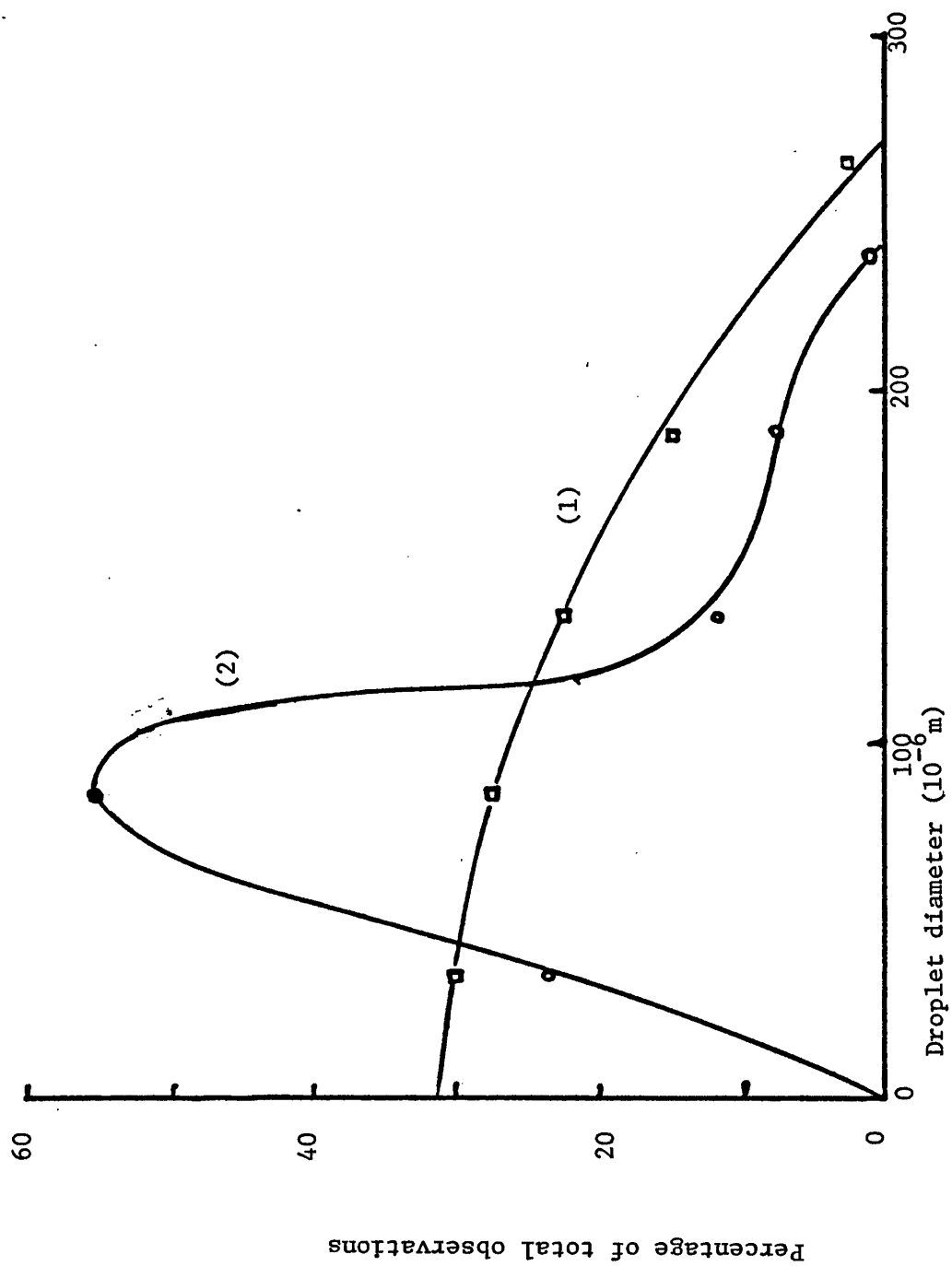


FIGURE 16. Droplet size distribution: (1) center of spray, (2) fringe of spray.

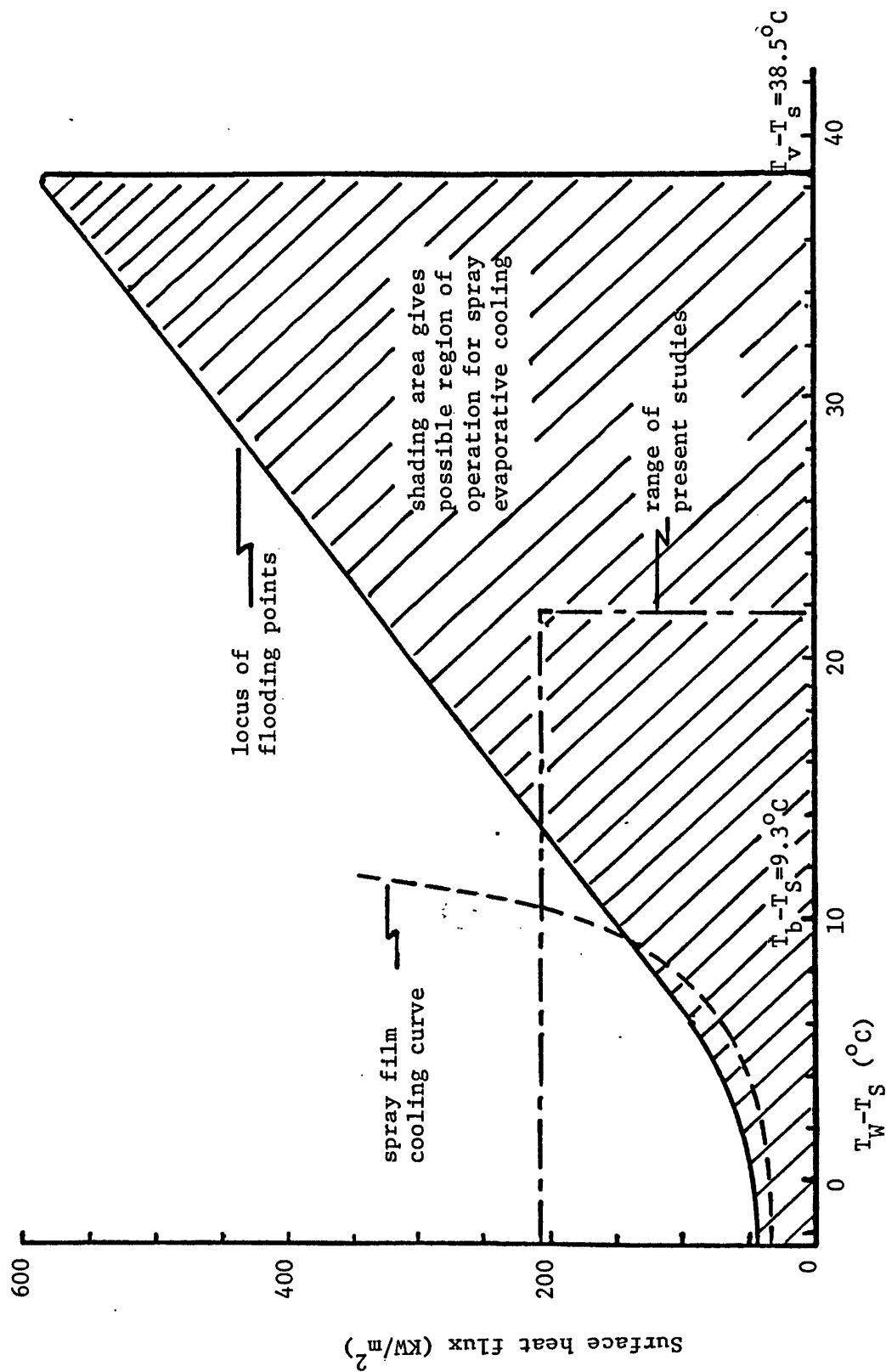


FIGURE 17. Overall spray evaporative cooling range at atmospheric pressure assuming continued droplet evaporation without internal boiling.

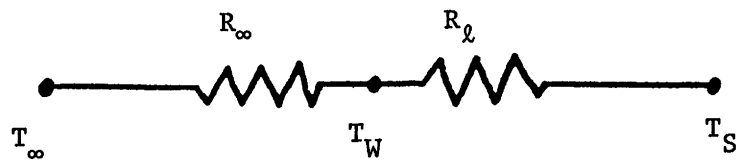
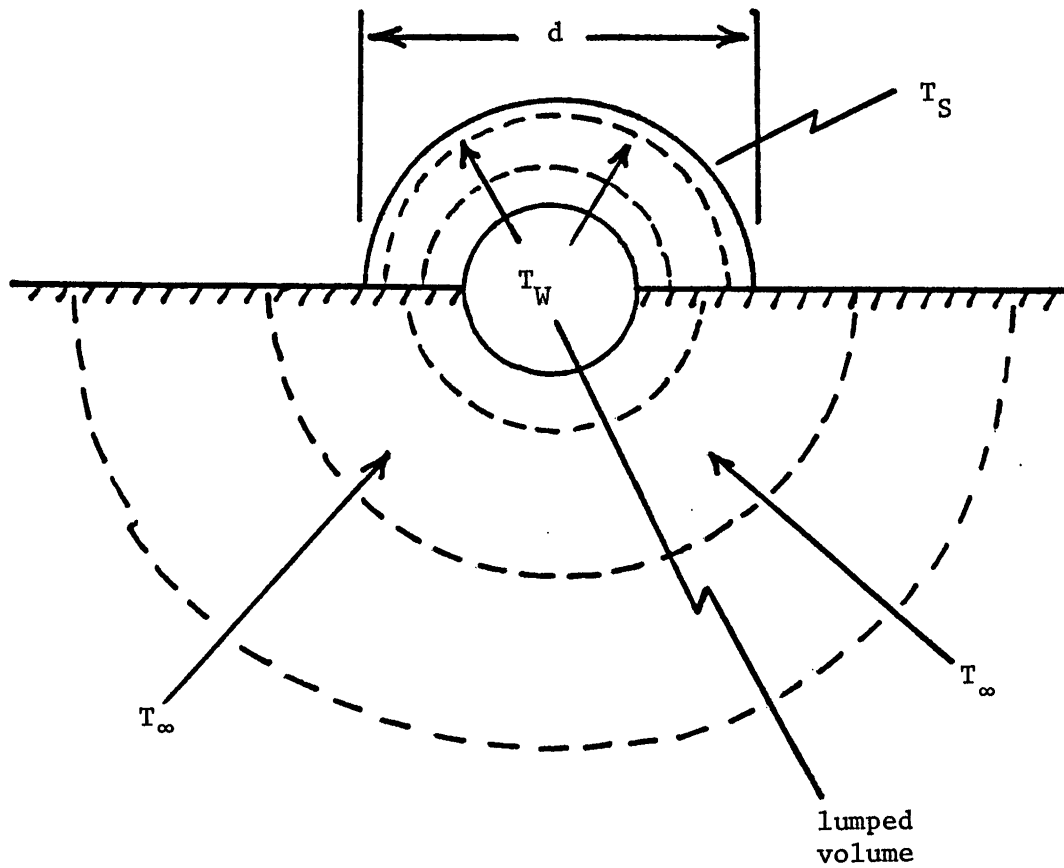


FIGURE 18. Simplified model for thermal conductivity analysis.

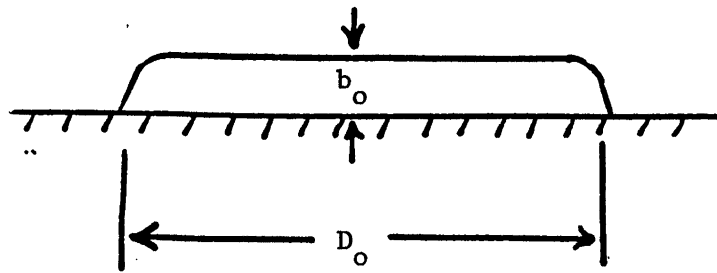


FIGURE 19. Initial droplet shape.

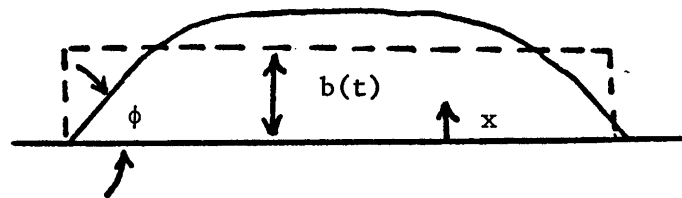


FIGURE 20. Droplet during second domain of evaporation.

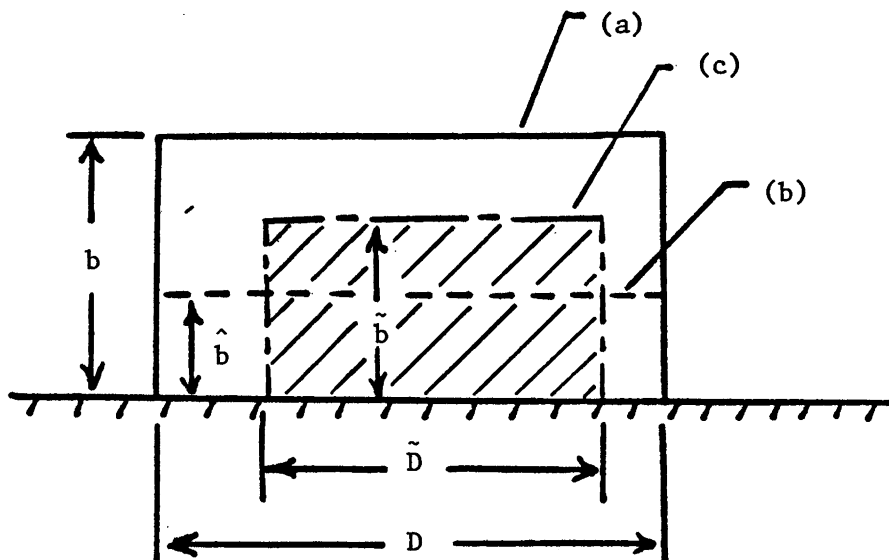


FIGURE 21. Effect of mass removal at droplet surface upon thickness.

/ G1 RELEASE 2.0

MAIN

DATE = 78331

21/16/05

EXTERNAL PARAB. INTERP

C

```

      DIMENSION T(150), EMF(150), PRESS(50), TEMP(50), X(15)
      DIMENSION DATA(150), E(15), P(150), TS1(150)
      DIMENSION EW(150), TW(150), TS(150), DEDX(150)
      DIMENSION DTDE(150), AUX(150)
80  FORMAT(F5.0,F5.3)
85  FORMAT(F6.5,F6.2)
90  FORMAT(F7.4,9(F5.3),F6.3,F5.1,F6.2)
95  FORMAT(1X,'INPUT',/,1X,I3,2X,'DATA=',F6.3,' EMF= ',
1   9(F2.0,'*',F5.3,1X),/,15X,' P=',F7.3,' TS1=',F5.1,' FLOW= ',
1   F5.1)
96  FORMAT(1X,'OUTPUT',/,1X,I3,3X,F10.3,5X,9(F2.0,'*',F5.3,1X),/,
1   116X,F7.3,4X,F5.1,' A=',F7.5,' B=',F7.5,' C=',E11.4,
1   ' NUMBER=', I3,/)
100 FORMAT(/, 1X,'FINAL OUTPUT',/,1X,I3,2X,'DATA=', F6.3,
1   ' TDEL=', F5.1,' Q=',E12.5,' TW=',F5.1,/,
1   10X,' COND=',F6.2,' DTDE=',F6.2,' TS=', F5.1,' HFG=',E14.7,
1   ' SPRAY=', E14.7)
110 FORMAT(20X,I4,5X, 'TEMP=',E14.7, 5X,'EMF=',E14.7,/)
120 FORMAT(20X,I4,5X, 'PRESS=',E14.7,5X, 'TEMP=',E14.7,/)

```

C

VARIABLES

C

C

C

C

C

C

C

C

C

C

C

C

C

C

C

C

C

C

C

C

C

C

C

C

C

C

C

C

C

C

C

C

C

C

C

C

C

C

C

C

C

C

C

C

C

C

T,EMF = TABULAR DATA

PRESS, TEMP = TABULAR PAIRS FOR SATURATED WATER

JEND = NUMBER OF T-EMF PAIRS

KEND = NUMBER OF PRESS-TEMP PAIRS

X = THERMOCOUPLE POSITION

DATA = DATA PT. NO.

E = THERMOCOUPLE VOLTAGE AT X

P = PRESSURE FOR DATA PT. MM HG ORIF 2,3 IN HG ORIF. 1

TS1 = SAT. EMP DEG. F

FLOW = FLOW RATE

A = PARABOLIC COEFF.

B = " "

C = " "

THEN E(X) = A+BX+CX**2

EW = THERMOCOUPLE VOLTAGE AT WALL

TW = TEMP AT WALL

AUX,AUX2 = TRANSFER MATRICES

DEDX = TEMP GRADIENT, UNITS MV PER 1/4 INCH

DTDE = MW TO TEMP CONVERSION AT WALL TEMP

COND = ALUMINUM CONDUCTIVITY AT WALL TEMP

Q = HEAT FLUX AT WALL

TDEL = DIFFERENCE BETWEEN WALL TEMP AND SAT TEMP

PARAB = LEAST SQUARES PARABOLIC SUBROUTINE

SPFIT = SPLINEFIT INTERPOLATION SUBROUTINE

ALL VARIABLES IN ENGLISH UNITS, IE. DEG. F, BTU, FT
 PRESSURES IN MM HG FOR ORIFICES 2 AND 3, IN IN HG FOR ORIFICE 1
 SATURATION TEMPERATURE INPUTS OVERRIDE PRESSURE MEASUREMENTS

READ IN TABULAR DATA FOR EMF=F(T) AND TS=F(P)

DO 10 J = 1,5000

Table 1. Data analysis computer program

G1 RELEASE 2.0

MAIN

DATE = 78331

21/16/05

```

      READ(5,80) T(J),EMF(J)
      WRITE(6,110) J,T(J),EMF(J)
      IF(T(J).EQ.0.) GO TO 20
10  CONTINUE
20  JEND = J+1
      DO 30 K=1,5000
      READ(5,85) PRESS(K), TEMP(K)
      WRITE(6,120) K,PRESS(K),TEMP(K)
      IF(PRESS(K).EQ.0.) GO TO 40
30  CONTINUE
40  KEND = K+1

C
C  READ IN DATA CARDS
C
      DO 50 I1=1,5000

C
C  RELATE THERMOCOUPLE READINGS TO POSITION X UNITS 1/4 INCHES
C
      DO 45 K2=1,9
      X(K2) = K2
45  CONTINUE
      READ(5,90) DATA(I1),(E(I2),I2=1,9),P(I1),TS1(I1),FLOW
      WRITE(6,95) I1,DATA(I1),(X(I2),E(I2),I2=1,9),P(I1),TS1(I1),FLOW
      IF(DATA(I1).EQ.0.) GO TO 60

C
      NUMBER = 9
      A = 0.
      B = 0.
      C = 0.

C
C  SHIFT NUMBERS DOWN ONE INDEX UNTIL ALL 0. READINGS ARE DISPLACED
C
      DO 46 I3=1,9
      IF(E(I3).GT.0.) GO TO 46
48  NUMBER = NUMBER+1
      IF(I3.GT.NUMBER) GO TO 49
      DO 47 I4=I3,NUMBER
      E(I4) = E(I4+1)
      X(I4) = X(I4+1)
47  CONTINUE
      IF(E(I3).GT.0.) GO TO 46
      GO TO 48
46  CONTINUE

C
49  CONTINUE
      USE THIS WRITE FOR DEBUGGING
      WRITE(6,96) I1,DATA(I1),(X(I2),E(I2),I2=1,9),P(I1),TS1(I1),
1  A,B,C, NUMBER

      ELIMINATE THERMOCOUPLE NO. 9 READING FOR MOST DATA PTS.

      IF(NUMBER.GT.5) NUMBER=NUMBER+1

C
C  SELECT CERTAIN DATA GROUPS FOR ANALYSIS, UNIT CONVERSION, ECT.
C
      CONVERT PRESSURES TO PSIA FOR INTERPOLATION IN STEAM TABLES
      FOR ZERO INPUT PRESSURE CONVERT TO .1 PSIA TO AVOID PROBLEMS

```

Table 1 (cont.)

V G1 RELEASE 2.0

MAIN

DATE = 78331

21/16/05

```

C      IN INTERPOLATION
C
C      IDATA = DATA(I1)
C      IF(IDATA.EQ. 4.OR.IDATA.EQ. 5) P(I1)=1.9337E=2*P(I1)
C      IF(IDATA.EQ.10.OR.IDATA.EQ.11) P(I1)=1.9337E=2*P(I1)
C      IF(IDATA.EQ.12.OR.IDATA.EQ.13) P(I1)=1.9337E=2*P(I1)
C      IF(IDATA.EQ.17.OR.IDATA.EQ.18) P(I1)=1.9337E=2*P(I1)
C      IF(IDATA.EQ. 3.OR.IDATA.EQ. 8) P(I1)=4.9116E=1*P(I1)
C      IF(IDATA.EQ.9 .OR.IDATA.EQ.16) P(I1)=4.9116E=1*P(I1)
C      IF(P(I1).EQ.0.) P(I1)=.1
C
C      CURVE FIT PARABOLA
C
C      CALL PARAB(X,E,NUMBER,A,B,C)
C
C      EW(I1) = A
C      DEDX(I1) = B
C
C      OUTPUT PRELIMINARY RESULTS
C
C      WRITE(6,96) I1,DATA(I1),(X(I2),E(I2),I2=1,9),P(I1),TS1(I1),
C      1 A,B,C, NUMBER
C
C      50 CONTINUE
C      60 IEND = I1=1
C
C      INTERPOLATE FOR TW IN THERMOCOUPLE TABLES AND DTDE AT T = TW
C
C      CALL INTERP(EMF,T,EW,TW,JEND,IEND,DTDE)
C
C      INTERPOLATE FOR TS IN STEAM TABLES
C
C      CALL INTERP(PRESS,TEMP,P,TS,KEND,IEND,AUX)
C
C      CALCULATE Q AND TDEL
C
C      DO 70 L=1,IEND
C
C      COND = 92.82 +8.184E=2*TW(L) = 4.144E=4*TW(L)**2
C      Q = 48.*COND*DEDX(L)*DTDE(L)
C      CONVERT TO KW/M2
C      Q = 3.155E=3*Q
C
C      CALCULATE MASS FLUX
C
C      HFG = 1075.8=.5977*(TS(L)=32.)
C      CONVERT TO J/G
C      HFG = 2.326*HFG
C      SPRAY FLUX CC/S=CM2
C      SPRAY = .1*Q/HFG
C      IF(TS1(L).GT.0.) TS(L)=TS1(L)
C      TDEL = TW(L)=TS(L)
C      CONVERT TO DEG C
C      TDEL = 1./1.8*TDEL
C      CONVERT TO KW/M=C
C      COND = 1.731E=3*COND

```

Table 1 (cont.)

G1 RELEASE 2.0

MAIN

DATE = 78331

21/16/05

C OUTPUT FINAL RESULTS

C

```

WRITE(6,100) L,DATA(L),TDEL,Q,TW(L),COND,DTDE(L),TS(L),HFG,SPRAY
70 CONTINUE
STOP
END

```

V G1 RELEASE 2.0

MAIN

DATE = 78331

21/16/05

C

```

SUBROUTINE INTERP(X,Y,XIN,YOUT,NO,IN,SLOPE)
DIMENSION X(NO), Y(NO), XIN(IN), YOUT(IN), SLOPE(IN)
40 FORMAT(//,40X,14.2X,'INPUT NO BOUNDED BY TABLE',//)
44 FORMAT(//,15X,'DATA PTS STRADDLED BY INTERPOLATION',//)
45 FORMAT(10X,14.2X,14.2X,'X(I)=', E14.7,2X, 'Y(I)=',E14.7,2X,
1 'X(I+1)=', E14.7,2X, 'Y(I+1)=', E14.7)
WRITE(6,44)

```

C

```

DO 10 J=1,IN
DO 20 I=1,NO
IF(I.EQ.NO) WRITE(6,40) J
IF(X(I+1).GT.XIN(J)) GO TO 30
20 CONTINUE

```

C

```

30 CONTINUE
SLOPE(J) = (Y(I+1)-Y(I))/(X(I+1)-X(I))
YOUT(J) = Y(I) + SLOPE(J)*(XIN(J)-X(I))
WRITE(6,45) J,I,X(I),Y(I),X(I+1),Y(I+1)
10 CONTINUE
RETURN
END

```

Table 1 (cont.)

IV G1 RELEASE 2.0

PARAB

DATE = 78331

21

```

      SUBROUTINE PARAB(X,Y,NO,C1,C2,C3)
C
C  2ND ORDER LEAST SQUARES FIT
C  VARIABLES
C  X = GIVEN VALUES FOR INDEPENDANT VARIABLE
C  Y = GIVEN VALUES FOR DEPENDANT VARIABLE
C  NO = NUMBER OF DATA POINTS
C  RETURNS = Y = F(X) = C1 + C2*X + C3*X**2
C
      DIMENSION X(NO), Y(NO)
C
C  EMPLOY SIMPLE LINEAR FIT FOR LESS THAN 3 DATA POINTS
C
      IF(NO.GT.3) GO TO 10
      C1 = (X(2)*Y(1)-X(1)*Y(2))/(X(2)-X(1))
      C2 = (Y(2)-Y(1))/(X(2)-X(1))
      C3 = 0.
      GO TO 25
C
C  INITIALIZE VARIABLES
C
10  A=0.
    B=0.
    C=0.
    D=0.
    E=0.
    F=0.
    G=0.
    P = NO
C
    DO 20 I = 1,NO
      A = A + X(I)
      B = B + X(I)**2
      C = C + X(I)**3
      D = D + X(I)**4
      E = E + Y(I)
      F = F + Y(I)*X(I)
      G = G + Y(I)*X(I)**2
    20 CONTINUE
C
      DEN=P*B*D+2.*A*B*C-B**3-P*C**2-D*A**2
      C1=(B*D*E+A*C*G+B*C*F-G*B**2-E*C**2-A*D*F)/DEN
      C2=(P*D*F+B*C*E+A*B*G-F*B**2-P*C*G-A*D*E)/DEN
      C3=(P*B*G+A*B*F+A*C*E-E*B**2-P*C*F-G*A**2)/DEN
C
25  CONTINUE
    RETURN
    END

```

Table 1 (cont.)

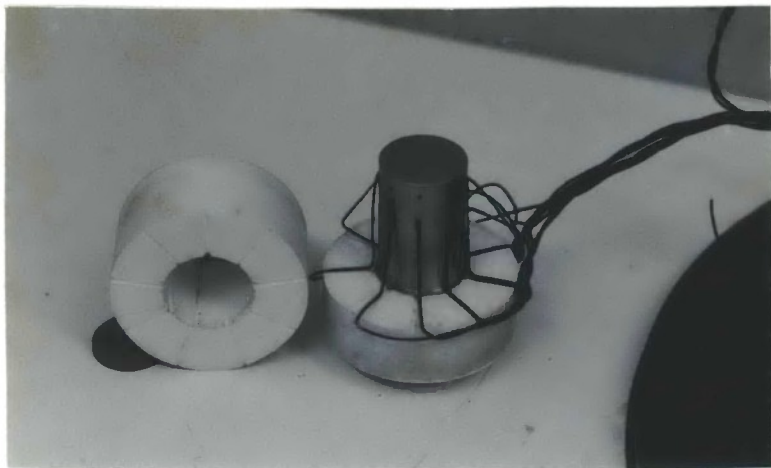


Photo 1.

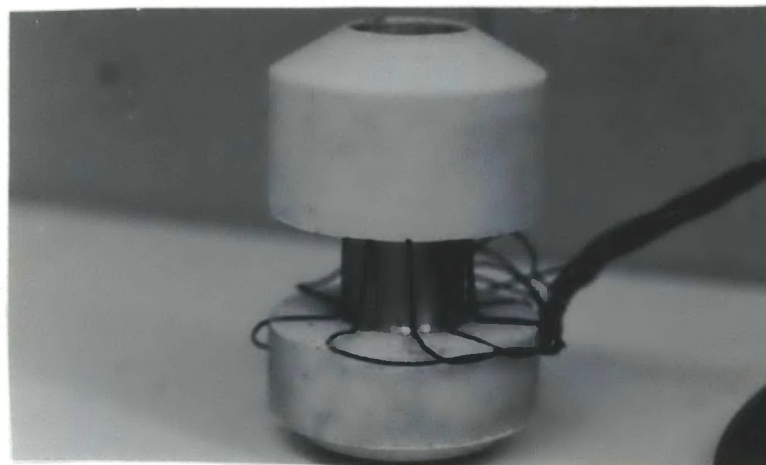


Photo 2.



Photo 3.



Photo 4.



Photo 5.



Photo 6.

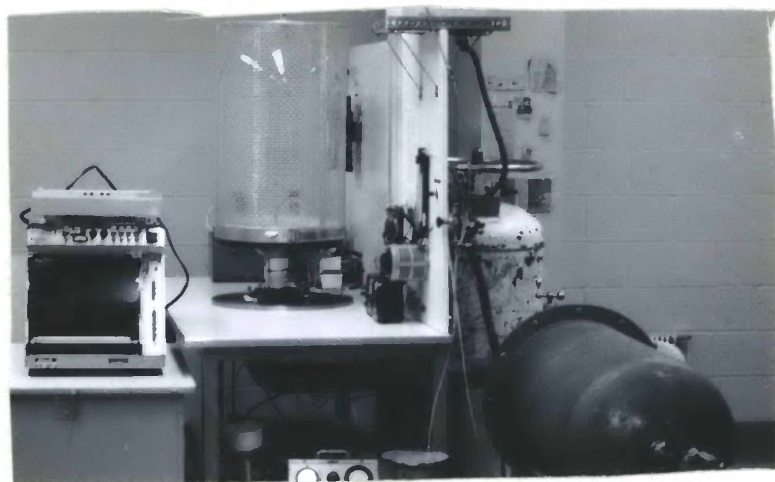


Photo 7.



Photo 8.